Nernst effect in high-T_c superconductors

Yayu Wang,* Lu Li,† and N. P. Ong‡
Department of Physics, Princeton University, Princeton, New Jersey 08544, USA
(Received 23 September 2005; revised manuscript received 23 November 2005; published 24 January 2006)

The observation of a large Nernst signal e_N in an extended region above the critical temperature T_c in hole-doped cuprates provides evidence that vortex excitations survive above T_c. The results support the scenario that superfluidity vanishes because long-range phase coherence is destroyed by thermally created vortices (in zero field) and that the pair condensate extends high into the pseudogap state in the underdoped (UD) regime. We present a series of measurements to high fields H which provide strong evidence for this phase-disordering scenario. Measurements of e_N in fields H up to 45 T reveal that the vortex Nernst signal has a characteristic "tilted-hill" profile, which is qualitatively distinct from that of quasiparticles. The hill profile, which is observed above and below T_c, underscores the continuity between the vortex-liquid state below T_c and the Nernst region above T_c. The upper critical field (depairing field) H_{c2} determined by the hill profile (in slightly UD to overdoped samples) displays an anomalously weak T dependence, which is consistent with the phase-disordering scenario. We contrast the Nernst results and H_{c2} behavior in hole-doped and electron-doped cuprates. Contour plots of $e_N(T,H)$ in the T-H plane clearly bring out the continuous extension of the low-T vortex liquid state into the high-T Nernst region in hole-doped cuprates (but not in the electron-doped cuprate). The existence of an enhanced diamagnetic magnetization M that survives to intense H above T_c is obtained from torque magnetometry. The observed M scales accurately like e_N above T_c, confirming that the large Nernst signal is associated with local diamagnetic supercurrents that persist above T_c. We emphasize implications of the new features in the phase diagram implied by the high-field results and discuss relevant theories.

DOI: 10.1103/PhysRevB.73.024510 PACS number(s): 74.40.+k, 72.15.Jf, 74.72.−h, 74.25.Fy

I. INTRODUCTION

In the quest to understand high-T_c superconductivity in the cuprates, two related important issues are the nature of the pseudogap state, which appears at the temperature T^*,[1–3] and the nature of the superconducting transition at the critical temperature T_c. Does the transition follow the familiar "gap-closing" BCS (Bardeen-Cooper-Schrieffer) scenario or the phase-disordering scenario in which thermally generated vortices destroy long-range phase coherence?[4] The former case would imply that the pseudogap state is inherently antagonistic to d-wave superconductivity and competes with it. In the latter case, by contrast, the pair condensate, bereft of phase rigidity, extends high above T_c into the pseudogap state. The two states are closely related, differing in a subtle way that is fundamental to the pairing mechanism.

The phase-disordering scenario, which lately has gained increased theoretical interest,[2–9] is a three-dimensional (3D) version of the well-known two-dimensional (2D) Kosterlitz-Thouless (KT) transition.[10–14] There are many investigations of KT physics in 2D cuprates realized in ultrathin films or superlattices.[15] A notable result is the detection of kinetic inductance above T_c at THz frequencies.[16]

In bulk cuprates, the Uemura plot[17] provided early evidence that T_c scales with the superfluid density inferred from muon spin relaxation (μSR), consistent with the phase disordering scenario. Direct evidence for this scenario has been obtained from Nernst experiments on single crystals.[18] When a flow of vortices is induced in a superconductor, an electric field appears transverse to the flow direction because of the Josephson effect.[19] The Nernst experiment, which exploits an unusual symmetry of the vortex-current response, is capable of detecting vorticity with high sensitivity. A large Nernst signal e_N extending from below T_c to a broad interval above has been detected in many hole-doped cuprates. The results have been interpreted as evidence for vortices existing above T_c and—by direct implication—the phase-disordering scenario.[18,20–24] See also Refs. 25 and 26.

In defining an extended region above the "T_c dome" in which vorticity exists (which we call the "Nernst region"), the Nernst results are increasingly influencing the ongoing pseudogap debate.[2,3,27–34] Nonetheless, acceptance of a vortex origin for e_N above T_c is by no means unanimous; several models interpreting the Nernst results strictly in terms of quasiparticles have appeared.[35–39] The difficulties may arise because the Nernst experiment is a relatively unfamiliar probe of superconductivity, with a checkered theoretical history.[40–43] Moreover, the notion that vortex excitations exist high above T_c in *bulk* samples goes against deeply entrenched ideas of the superconducting state derived from BCS superconductors. In this paper, we lay out in some detail the reasoning and evidence that have guided our thinking, with focus on recent measurements in intense fields.

The organization of the paper is as follows. Section II explains our notation and concepts relevant to the vortex-Nernst effect. Section III sketches the phase-disordering scenario and the role of singular phase fluctuations. In Secs. IV and V, we give an introductory overview of Nernst results on optimally doped and underdoped cuprates, respectively. Section VI describes the characteristic hill profile of the vortex signal and the continuity of the vortex liquid phase across T_c, while Sec. VII discusses the anomalous T dependence of the depairing field H_{c2}. The phase diagram is discussed in Sec. VIII. Recent corroboration of this interpretation from magnetization is summarized in Sec. IX. Nernst results in the

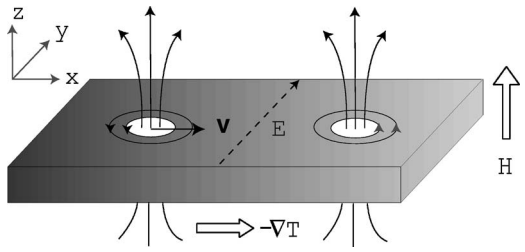

FIG. 1. The vortex-Nernst effect in a type-II superconductor. Concentric circles represent vortices.

electron-doped cuprate are described in Sec. X. Theoretical issues are surveyed in Sec. XI. Finally, in Sec. XII we summarize the results and conclusions.

The standard acronyms are used to identify the cuprates: LSCO for $La_{2-x}Sr_xCuO_4$, Bi 2201 for $Bi_2Sr_{2-y}La_yCuO_6$, Bi 2212 for $Bi_2Sr_2CaCu_2O_{8+\delta}$, Bi 2223 for $Bi_2Sr_2Ca_2Cu_3O_{10+\delta}$, YBCO for $YBa_2Cu_3O_y$, and NCCO for $Nd_{2-x}Ce_xCuO_4$. For brevity, qp, UD, OP, and OV stand for quasiparticle, underdoped, optimally doped, and overdoped, respectively. Where necessary, we distinguish vortex and qp terms by the superscripts "*s*" and "*n*," respectively.

II. VORTEX-NERNST EXPERIMENT

The Nernst effect in a solid is the detection of an electric field $\mathbf{E}$ (along $\pm\hat{\mathbf{y}}$, say) when a temperature gradient $-\boldsymbol{\nabla}T||\hat{\mathbf{x}}$ is applied in the presence of a magnetic field $\mathbf{H}||\hat{\mathbf{z}}$ ($\mathbf{E}$ is antisymmetric in $\mathbf{H}$). The Nernst *signal*, defined as E per unit gradient—viz., $e_N(H,T)=E/|\boldsymbol{\nabla}T|$—is generally much larger in ferromagnets and superconductors than in nonmagnetic normal metals. Where e_N is linear in H (conventional metals), it is customary to define the Nernst coefficient $\nu=e_N/B$ with $B=\mu_0 H$. Our focus here, however, is on the vortex-Nernst effect in type-II superconductors, where e_N is intrinsically strongly nonlinear in H. Instead of ν, it is more useful for our purpose to discuss the Nernst signal $e_N(T,H)$.

We remark that, to produce in a ferromagnetic conductor a signal e_N of the magnitude reported here ($\sim 0.1-1$ μV/K), one would need a magnetization M of 10^4-10^5 A/m.[44] This is very far from the case in cuprates, where $|M|=5-50$ A/m in the Nernst region. Hereafter, we focus on the vortex mechanism.

In the vortex-liquid state, a gradient $-\boldsymbol{\nabla}T$ drives the vortices to the cooler end of the sample because a normal vortex core has a finite amount of entropy relative to the zero-entropy condensate (Fig. 1).[19,45,46] Because of the 2π phase singularity at each vortex core, vortex motion induces phase slippage.[47] By the Josephson equation $2eV_J=\hbar\dot{\theta}$, the time derivative of the phase $\dot{\theta}$ produces an electrochemical potential difference V_J. We have $\dot{\theta}=2\pi\dot{N}_v$, where $\dot{N}_v$ is the number of vortices crossing a line $||\hat{\mathbf{y}}$ per second. The Josephson voltage V_J may be expressed as a transverse electric field $\mathbf{E}=\mathbf{B}\times\mathbf{v}$ which is detected as the Nernst signal.

The peculiar symmetry here, in which a driving force along $\hat{\mathbf{x}}$ produces—as the leading response—a conjugate current along $\hat{\mathbf{y}}$ that is antisymmetric in $\mathbf{H}$, is specific to vortex currents. The Nernst effect is particularly suited to its observation. The sign of the Nernst signal is not intrinsically related to the sign of a charge (unlike the Hall effect). Fortunately, the Josephson equation, which dictates that $\mathbf{E}||\mathbf{H}\times(-\boldsymbol{\nabla}T)$, provides a sign convention for the Nernst experiment.[20] We regard the Nernst signal as positive if it is consistent with vortex flow.

Generally, because e_N is difficult to calculate from a microscopic model, a phenomenological description is often used.[19,45,46] The force exerted by the gradient on the vortex (per unit length) is $\mathbf{f}=s_\phi(-\boldsymbol{\nabla}T)$ where s_ϕ is called the "transport entropy" (per length). Balancing this against the frictional force in steady state, we have $\eta\mathbf{v}=s_\phi(-\boldsymbol{\nabla}T)$, where the damping viscosity η may be inferred from the flux-flow resistivity $\rho=B\phi_0/\eta$ with $\phi_0=h/2e$ the superconducting flux quantum. The Nernst signal is then

$$e_N=\frac{Bs_\phi}{\eta}=\frac{\rho s_\phi}{\phi_0}. \tag{1}$$

We may extract s_ϕ by measuring e_N and ρ, but now all the difficulties attendant to e_N reside in s_ϕ.

[In the vortex solid state (when H is below the melting field H_m), the force due to the gradient $\mathbf{f}$ is too feeble to cause vortex motion and e_N is rigorously zero. In low-T_c type-II superconductors, it is more practical to employ the Ettingshausen effect,[19] which is related to the Nernst effect by reciprocity. In the Ettingshausen experiment, a current density $\mathbf{J}$ is applied $||\hat{\mathbf{x}}$ with $\mathbf{H}||\hat{\mathbf{z}}$. Vortex motion transverse to $\mathbf{J}$ produces a heat current which leads to a gradient $\boldsymbol{\nabla}T||\hat{\mathbf{y}}$ detected as the Ettingshausen signal. The Ettingshausen coefficient is $\mathcal{Q}_E=|\boldsymbol{\nabla}T|/JH$. The advantage of the Ettingshausen experiment is that a large $\mathbf{J}$ may be used to depin the vortex lattice below H_m.[45,48]]

In theoretical treatments, the vortex Nernst and Ettingshausen effects are conveniently handled together as the current response of the system to $\mathbf{E}$ and $-\boldsymbol{\nabla}T$.[40–43] Imagine that we apply to a vortex system mutually orthogonal E field and temperature gradient in the plane normal to $\mathbf{H}$, and observe the response of the charge and heat current densities $\mathbf{J}$ and $\mathbf{J}^h$, respectively. As mentioned, the peculiar symmetry of vortex currents dictates that $\mathbf{J}$ is $\perp$ to $-\boldsymbol{\nabla}T$ but $||\mathbf{E}$, whereas $\mathbf{J}^h$ is $\perp$ to $\mathbf{E}$ but $||(-\boldsymbol{\nabla}T)$. (These are the *large* current responses; the flux-flow Hall effect and thermopower related to vortex diffusion produce much weaker currents which we neglect, along with qp contributions.)

In linear response, $\mathbf{J}$ and $\mathbf{J}^h$ are given by[40,42]

$$J_y=\sigma E+\alpha_{yx}^s(-\partial T), \tag{2}$$

$$J_x^h=\tilde{\alpha}_{xy}^s E+\kappa(-\partial T), \tag{3}$$

with $\mathbf{E}||\hat{\mathbf{y}}$, $-\boldsymbol{\nabla}T||\hat{\mathbf{x}}$. Here $\sigma=1/\rho$ and κ is the thermal conductivity. The two off-diagonal Peltier terms are related by $T\alpha_{xy}^s=\tilde{\alpha}_{xy}^s$ by Onsager reciprocity. Setting J to zero, we find that

$$e_N=\rho\alpha_{xy}^s, \tag{4}$$

which is to be compared with Eq. (1). Similarly with $J^h=0$, the Ettingshausen coefficient is $\mathcal{Q}_E=\tilde{\alpha}_{xy}^s/H\sigma\kappa$.

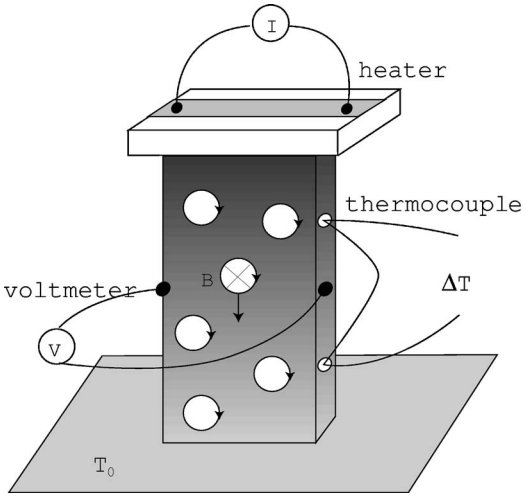

FIG. 2. Crystal mounting geometry in the Nernst experiment.

In a Hartree-Fock approximation, Caroli and Maki[40,41] found that α_{xy}^s is proportional to the magnetization M for H close to H_{c2} and $T \to T_c$. Their coefficient of proportionality had an error which was later corrected.[42,43] Here we express this relationship as

$$\alpha_{xy}^s = \tilde{\beta} M \quad (H \to H_{c2}^-), \tag{5}$$

with the parameter $\tilde{\beta}$ to be determined by experiment ($\tilde{\beta}$ has dimensions of $1/T$).

The charge carriers also produce a Nernst signal which we refer to as the quasiparticle contribution. The current density produced by an applied gradient is given by the Peltier tensor α_{ij}^n—viz., $J_i = \alpha_{ij}^n(-\partial_j T)$. In terms of α_{ij}^n and the Hall resistivity ρ_{xy}^n, the qp Nernst signal is[20]

$$e_N^n = \rho^n \alpha_{xy}^n - \rho_{xy}^n \alpha^n, \tag{6}$$

where ρ^n is the qp resistivity and $\alpha^n \equiv \alpha_{xx}^n$ is related to the thermopower by $S = \rho^n \alpha^n$.

The observed Nernst signal is the sum of the vortex and qp terms—viz.,

$$e_N = e_N^s + e_N^n, \tag{7}$$

with the caveat that in Eq. (6) for e_N^n, the total (observed) ρ, α, and ρ_{xy} are used instead of the strictly qp terms.

In the hole-doped cuprates, the qp term is very small for $T < T_c$. For the purpose of determining the onset temperature T_{onset} of e_N^s, however, the qp term has to be carefully resolved. This involves measuring the thermopower $S = \rho\alpha$, Hall angle $\tan\theta = \rho_{xy}/\rho$, and resistivity ρ in addition to e_N. As this procedure has been described in detail in Ref. 20, we will not repeat it here. In what follows, we will not usually distinguish between e_N and e_N^s, except when discussing NCCO in Sec. X.

Figure 2 shows the setup in our Nernst experiment. The samples used are high-quality cuprate single crystals of typical size of $1.2 \times 0.8 \times 0.05$ mm^3. One end of the crystal is glued with silver epoxy onto a sapphire substrate, which is heat-sunk to a copper cold finger. A thin-film 1 kΩ heater, silver-epoxied to the top edge of the crystal, generates the heat current flowing in the *ab* plane of the crystal. The temperature difference ΔT (0.3–0.5 K) is measured by a pair of fine-gauge Chromel-Alumel thermocouples. A pair of Ohmic contacts are prepared on the edge of the sample by annealing different kinds of conductive materials.

After the bath temperature is stabilized (to within ±10 mK), the gradient is turned on. The Nernst voltage is preamplified and measured by a nanovoltmeter as the magnetic field is slowly ramped up. The uncertainty in V is ±5 nV. To remove stray longitudinal signals due to misalignment of the contacts, the magnetic field is swept in both directions. Only the field-asymmetric part of the raw data is taken as the Nernst signal.

As expressed in Eq. (7), the Nernst signal is comprised of a large component e_N^s associated with the pair condensate and a qp component e_N^n from carriers. To date, the existence of e_N^s in the Nernst region above T_c has been confirmed in Bi 2212, Bi 2223, LSCO and YBCO, and $Bi_2Sr_{2-y}La_yCuO_6$ (Bi 2201). The interesting case of electron-doped $Nd_{2-x}Ce_xCuO_4$ (NCCO) is deferred to Sec. X.

III. VORTICES AND PHASE-DISORDERING TRANSITION AT T_c

In this section, we sketch the phase-disordering scenario associated with the appearance of thermally created vortices, which has heavily informed the analyses of our Nernst-effect experiments. In the superconducting state, the pair condensate described by the macroscopic wave function $\hat{\Psi} = |\Psi| e^{i\theta}$ exhibits long-range phase coherence. The phase spontaneously selects a particular value which is rigidly maintained throughout the volume.[47,49] The energy cost of local variations in $\theta(\mathbf{r})$ is given by $H_\theta = \frac{1}{2}\int d^2 r K_s (\nabla\theta)^2$, where the phase stiffness $K_s = \hbar^2 n_s / 4m^*$ arises from the kinetic energy of the superfluid electrons, with n_s the 2D density and m^* the effective mass.[14]

In the Kosterlitz-Thouless problem[10–14]—the prototypical example of the phase-disordering scenario—vortex-antivortex unbinding at the KT transition temperature T_{KT} destroys long-range phase coherence and superfluidity, even though the pair amplitude $|\Psi|$ remains finite. Random 2π jumps in $\theta(\mathbf{r})$ caused by (anti)vortex motion drive the thermally averaged order parameter to zero—viz.,

$$\langle \hat{\Psi}(\mathbf{r}) \rangle = |\Psi| \langle e^{i\theta(\mathbf{r})} \rangle = 0. \tag{8}$$

Generally, the phase-disordering transition T_θ is proportional to the superfluid stiffness—viz.,[2,4,14]

$$k_B T_\theta = \mathcal{A}_1 K_s(T). \tag{9}$$

The dimensionless parameter $\mathcal{A}_1$ has been investigated in detail (see tabulation in Ref. 50). In the KT problem $\mathcal{A}_1 = \pi/2$ if K_s is evaluated at T_{KT}^-. In the 2D XY model on a square lattice, $\mathcal{A}_1 = 0.9$ if K_s is evaluated at $T = 0$. For the 3D XY model on a cubic lattice with intralayer (interlayer) exchange J ($J_\perp$), $\mathcal{A}_1$ varies from 0.9 ($J_\perp \ll J$) to 2.4 ($J_\perp = J$).

From μSR experiments, Uemura and collaborators[17] found that, in UD cuprates, T_c follows a universal, linear dependence on n_s/m^*. Although originally discussed in terms

of boson condensation at T_c, the Uemura plot—if reinterpreted as confirming Eq. (9)—provided initial evidence for the phase-disordering scenario. Very early, Baskaran *et al.*[5] and Doniach and Inui[6] noted that proximity to the Mott insulator implies that T_c in UD cuprates must be controlled by loss of phase coherence. The first detailed examination of this issue was provided by Emery and Kivelson[4] who found that the ratio K_s/k_BT_c falls in the range 1–2 in most hole-doped cuprates (compared with 10^3-10^5 in low-T_c superconductors). This implies that phase fluctuations are of crucial importance in determining T_c. Corson *et al.*[16] measured the complex conductivity $\hat{\sigma}(\omega)$ in two thin-film samples of Bi 2212 with $T_c=74$ K and 33 K at THz frequencies and found that the kinetic inductance persists to ~25 K above T_c in both samples.

Fluctuations in θ are of two types: analytical spin-wave fluctuations $\Delta\theta_a$ and singular vortex-induced fluctuations $\Delta\theta_v$.[11] The singular fluctuations $\Delta\theta_v$ are of specific interest here.

As T rises above T_{KT}, the density of spontaneous vortices (antivortices) n_+ (n_-) increases exponentially but the net vorticity n_+-n_- stays at zero if $\mathbf{H}=\mathbf{0}$. The applied $\mathbf{H}$ increases n_+ (say) to produce a net induction field $B=(n_+-n_-)\phi_0$.[13] A detailed calculation of the KT magnetization $M=B\mu_0^{-1}-H$ over a broad interval of T was recently reported.[51] Above T_{KT}, both M and the vorticity remain observable despite the vanishing of $\langle\hat{\Psi}(\mathbf{r})\rangle$.

It is worth emphasizing that a weak interlayer coupling $J_\perp$ can make the KT physics very difficult to see close to T_{KT}. The 3D transition occurs above the KT transition by an amount[52]

$$\Delta T_c = T_{KT}\left[\frac{\pi}{\ln(1/\sqrt{J_\perp/J})}\right]^2. \tag{10}$$

Nonetheless, over a broad interval above T_c, KT physics may be probed by high-resolution susceptibility (see Li *et al.*[53] for recent magnetization measurements in Bi 2212).

In experimental studies of the KT transition in layered ferromagnets [e.g., K_2CuF_4 (Ref. 54)], the KT transition is preempted at $T_c>T_{KT}$ by a 3D Curie transition because of a weak interlayer exchange $J_\perp$ ($J_\perp \ll J$, the intralayer exchange). Nevertheless, over a broad interval above T_C, KT physics prevails. Analogously, in bulk cuprates, we expect the weak interlayer coupling to induce a 3D transition that preempts the KT transition. However, the KT description of vortex proliferation is valid over a broad interval above T_c (the Nernst region).

Close to T_c, the 3D *XY* model is the appropriate description for bulk crystals. Extensive numerical simulations by Nguyen and Sudbø[55] of the 3D *XY* model with moderate anisotropy $\alpha_J=J_\perp/J\sim\frac{1}{3}$ clearly show that the helicity modulus $\Upsilon=(\hbar/m)^2\rho_s$ (where ρ_s is the superfluid density) is destroyed at T_c by the spontaneous appearance of vortex loops. Even with $\alpha_J\sim\frac{1}{3}$, the simulations show a ~10 K interval above T_c where vorticity exists. These results were tentatively compared with YBCO, but simulations in the limit $1/\alpha\gg 1$ are desirable.

In the Nernst experiment, the flow of vortices and antivortices down the gradient generates signals of opposite signs. Hence the observed e_N^s picks up the difference in population n_+-n_-—i.e., the vorticity.

In the BCS scenario, fluctuations of the order parameter $\hat{\Psi}$ are (predominantly) fluctuations of the amplitude $|\Psi|$ (from zero). The Gaussian approximation, in which only terms in $|\Psi(\mathbf{x})|^2$ are retained in the action S of the partition function $\mathcal{Z}$, provides a good description of fluctuation diamagnetism measured in low-T_c superconductors.[56] However, if singular phase fluctuations $\Delta\theta_v$ are dominant in the destruction of superfluidity (as the evidence shows is appropriate in the Nernst region), the valid description is inherently non-Gaussian.

IV. OPTIMALLY DOPED CUPRATES

In the cuprates, early Nernst[57–59] and Ettingshausen[60] experiments were restricted to OP, bilayer cuprates. The results were largely confined to the vortex-liquid state below T_c, and analyzed to extract vortex parameters such as s_ϕ [Eq. (1)]. However, the existence of unusually large "fluctuation signals" extending 10–20 K above T_c was noted in OP Bi 2212 and YBCO.[57,60]

We start the description of our data from the OV-OP end of the doping window. Figure 3(a) displays the traces of e_N versus H at fixed T, in a crystal of $YBa_2Cu_3O_y$ (YBCO), with $y=6.99$ and $T_c=92.0$ K (this sample is slightly OV). As the melting field H_m is exceeded, the abrupt motion of a large number of vortices leads to a nearly vertical rise in e_N [panel (a)]. The signal reaches a broad maximum and then decreases slowly. The envelope of all these curves represents the maximum value that e_N attains in the temperature interval shown.

As T rises above T_c, the maximum values of $e_N(T)$ decrease markedly and the profiles become broader [panel (b)]. However, an abrupt transition is not observed in the Nernst signal. Instead, it retains its nonlinearity up to ~105 K. This is analogous to the Ettingshausen fluctuation signal reported in OP YBCO.[60] Above 110 K, the curve of e_N is linear in H with a slope that changes mildly with T, which we identify with the qp contribution e_N^n.

To show the fluctuation regime more clearly, we plot the T dependence of e_N measured at 14 T (Fig. 4) together with its zero-field resistivity ρ. Clearly, e_N deviates from the qp background at ~107 K, or 15 K above $T_c=92$ K. Similar measurements on OP bilayer $Bi_2Sr_2CaCu_2O_{8+\delta}$ (Bi 2212, $T_c=91$ K) are shown in Fig. 5(a). Owing to its extreme anisotropy, the vortex solid in Bi 2212 has a very small shear modulus c_{66}. The melting field H_m remains small even as $T\ll T_c$ (~50 K). We also remark that, near T_c, e_N displays a nonanalytic H dependence in weak H. Above T_c, e_N rapidly becomes much smaller in amplitude. Figure 5(b) displays the T dependence of e_N measured at 14 T together with the Meissner signal measured at $H=10$ Oe in a superconducting quantum interference device (SQUID) magnetometer. The onset temperature T_{onset} of the vortex-Nernst signal is ~125 K, or 30 K above T_c. The broader Nernst region in Bi

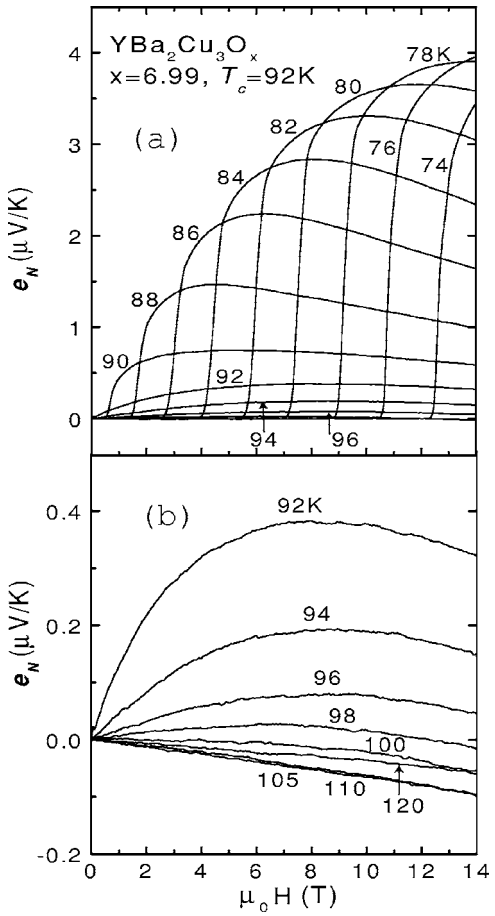

FIG. 3. Curves of the Nernst signal e_N vs H measured in slightly OV YBCO (x=6.99, T_c=92 K) at temperatures below T_c [panel (a)] and above T_c [panel (b)]. Below T_c, e_N rises nearly vertically at the melting field H_m. Above T_c (b), the negative H-linear contribution of the qp term e_N^n becomes quite apparent.

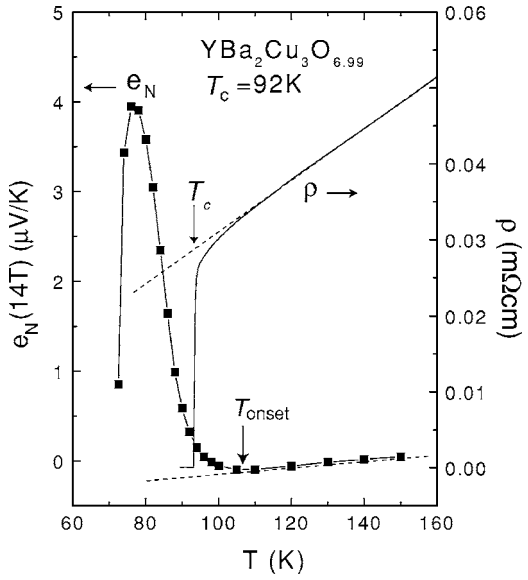

FIG. 4. Temperature dependence of e_N measured at 14 T compared with the resistivity ρ measured on OV YBCO (x=6.99, T_c=92 K). The onset temperature T_{onset} and T_c are indicated by arrows. The dashed line indicates the negative qp contribution.

2212 (compared to OP YBCO) reflects its extreme anisotropy.

The trilayer cuprate $Bi_2Sr_2Ca_2Cu_3O_{10+\delta}$ (Bi-2223) also shows similar extension of the Nernst signal above its T_c=109 K [Fig. 6(a)]. The overall behavior of e_N vs H is strikingly similar to that of the bilayer system [Fig. 5(a)]. The plots in Fig. 6(b) show that the Nernst onset temperature is around 135 K, ~25 K above the T_c.

The early results on OP cuprates in the "fluctuation" regime[57,60] were deemed compatible with the prevailing expectation that, although fluctuations are strongly enhanced in cuprates,[61] the data appeared to be adequately described by conventional Gaussian fluctuation theory.[62,63]

V. UNDERDOPED CUPRATES

The Nernst signal above T_c, already considerable in OP cuprates, becomes even larger in the UD regime. We first discuss $La_{2-x}Sr_xCuO_4$ (LSCO).[18] Figure 7(a) displays the Nernst traces in an UD crystal with x=0.12 and T_c=28.9 K. The results seem quite similar to that in optimally doped YBCO (Fig. 3). Below T_c, the curves, which display the characteristic profile of a "tilted hill" associated with vortex motion, are all enclosed within a smooth envelope curve. On closer examination, however, the data reveal an important difference. In OP YBCO, the maximum value of the e_N-H curve taken at T_c=92 K is ~0.38 μV/K, less than 10% the maximum value attained by the envelope curve ($\geq 4\mu$V/K) below T_c. Above T_c, e_N rapidly falls to a negligible fraction of 4 μV/K. By contrast, UD LSCO shows a different pattern of behavior. The bold curve in Fig. 7(a) is taken at T=30 K, slightly higher than T_c. Its value at 14 T, ~4 μV/K, is more than 50% of the maximum of the envelope and still increasing with field. Even at 50 K, more than 20 K above T_c, the signal is a sizable fraction of the maximum envelope value. A pronounced nonlinearity in the field is apparent in these curves. The Nernst signal decays quite slowly with temperature, becoming indistinguishable from the qp Nernst signal only above 100 K.

Figure 7(b) displays the T dependence of e_N taken at 14 T on underdoped LSCO, x=0.12, together with the magnetization curve measured at 10 Oe. The anomalous Nernst signal starts to deviate from the small qp background at T_{onset}~120 K. The T dependence of e_N measured at 14 T shows a long "fluctuation" tail that extends to T_{onset}.

Moving to LSCO with smaller x (0.07, T_c=11 K), we find that these anomalous features become enhanced (Fig. 8). The curve at T=12 K—1 K above T_c—displays a Nernst signal that is similar in overall magnitude to any of the curves below T_c. Indeed, curves taken at 20 K are comparable in magnitude with many of those below T_c. Similar results have been obtained by Capan *et al.*[25] Hence, from the perspective of the Nernst effect, the boundary between the superconducting state and the normal state in UD cuprates is truly blurred. This poses a serious challenge to the conventional notion of "fluctuations."

We next turn to the underdoped Bi 2212, which has been intensively studied by angle-resolved photoemission spec-

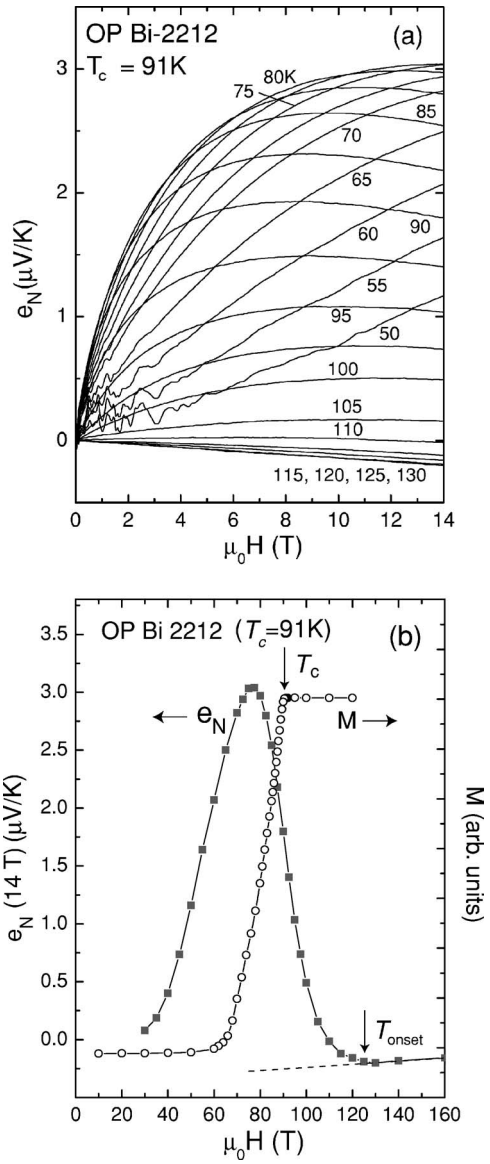

FIG. 5. (a) The Nernst signal e_N vs H in OP Bi 2212 (T_c=91 K) at temperatures 50–130 K. The oscillations in e_N in weak H are reproducible and may be caused by plastic flow of the vortices. (b) The T dependence of e_N measured at 14 T (solid squares) and the Meissner curve (magnetization M measured at H=10 Oe) in OP Bi 2212. The dashed line indicates the estimated negative qp contribution.

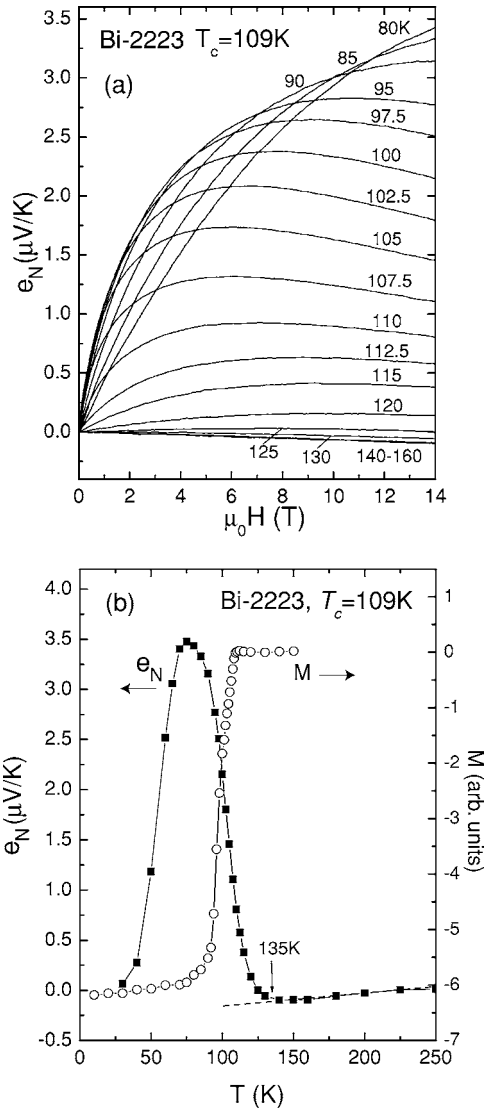

FIG. 6. (a) Curves of e_N vs H in OP Bi 2223 (T_c=109 K) measured at selected T. (b) The T dependence of e_N at 14 T compared with the Meisnner curve (M measured at 10 Oe) in OP Bi 2223. Dashed line is the negative qp contribution.

troscopy[64,65] (ARPES) and scanning tunneling microscopy[66,67] (STM) because the crystals can be cleaved cleanly. Nernst results on this system are particularly valuable. In Fig. 9, we show Nernst results on a very underdoped Bi 2212 crystal with T_c=50 K and hole density $x \sim 0.09$. In close similarity with very underdoped LSCO (x=0.07), the curve measured at T_c (bold line) has a peak value close to the maximum of the envelope [Fig. 9(a)]. Traces taken at T higher than T_c remain very large in magnitude and possess the strong curvature characteristic of the vortex state. An important feature of Bi 2212, both UD and OP, is the very small magnitude of the qp Nernst signal (the "background"). This allows the onset temperature T_{onset} to be determined unambiguously. The T dependence of e_N in this UD sample indicates that T_{onset}=118 K, or about 65 K above T_c [Fig. 9(b)].

VI. VORTEX-NERNST PROFILE AND CONTINUITY ACROSS T_c

As described in Secs. IV and V, the vortex-Nernst signal versus H displays a characteristic peaked form which we call a "tilted-hill" profile. This is quite apparent in electron-doped NCCO where the depairing field (10 T) is readily attained (Sec. X).[22] In hole-doped cuprates, however, H_{c2} is very large. The maximum field employed (14 T) in earlier experiments was barely enough to reach the peak of the profile. More recent measurements to fields of 45 T now provide a more complete view of the hill profile in Bi 2201 and LSCO. The similarity with the profile in NCCO is striking.

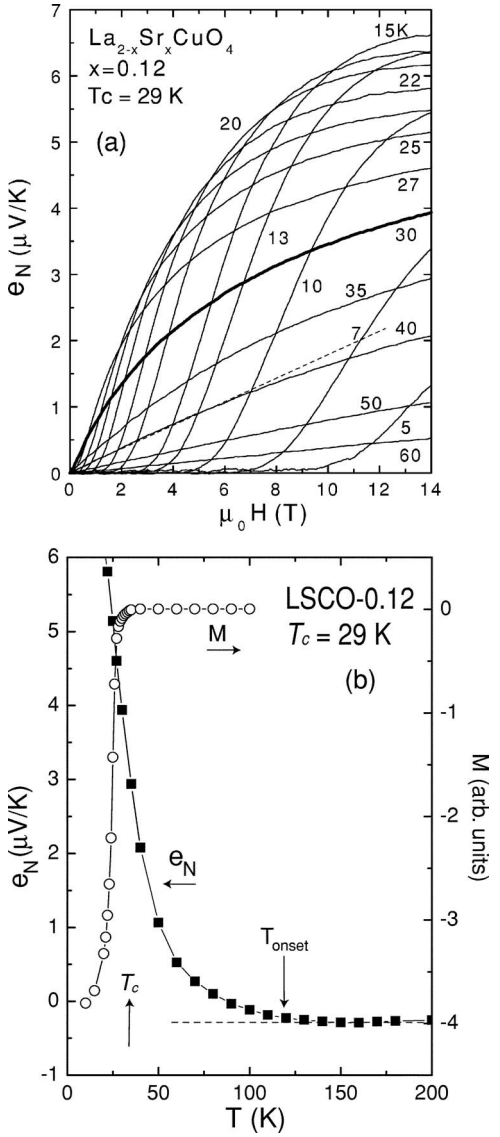

FIG. 7. (a) Curves of e_N vs H in UD LSCO (x=0.12, T_c=29 K). The bold curve is nominally at T_c. The dashed line at 40 K gives the initial slope used to find ν. (b) The T dependence of e_N measured at 14 T in UD LSCO (solid squares) compared with the Meissner curve (M measured at 10 Oe, open circles). Dashed line is the negative qp contribution.

As discussed, e_N rises steeply when H exceeds H_m. The vanishing of the shear modulus c_{66} in the vortex solid allows the vortices to move down the gradient $-\nabla T$, to generate the Nernst signal as discussed in Sec. II. The steep rise in e_N above H_m is primarily driven by the increase in vortex velocity $\mathbf{v}$, but also reflects the increase in the vortex density n_v. However, with increasing H, the magnitude of the magnetization M decreases monotonically as $M \sim -\ln H$ over a broad interval of field above the lower critical field H_{c1}. In high fields, $|M|$ decreases to zero at the upper critical field H_{c2}, as $|M| \sim (H_{c2}-H)$ (see Sec. VII). From Eq. (5), α_{xy}^s should scale like M in high fields,[40] so that it should also approach zero as $\sim(H_{c2}-H)$. Combining the weak-field and high-field trends, we may understand the tilted-hill profile. Just above H_m, the steep increase of $\mathbf{v}$ in the liquid state leads

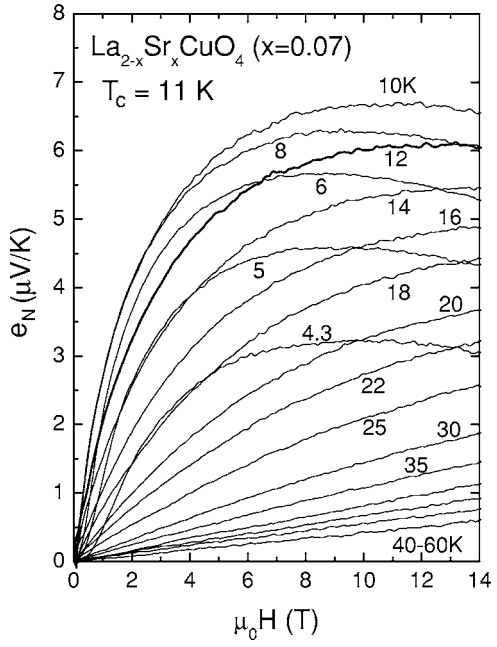

FIG. 8. Curves of e_N vs H in heavily UD LSCO (x=0.07, T_c=11 K). The bold curve is taken at 12 K, 1 K above T_c.

to a rapid increase in e_N until α_{xy}^s encounters the ceiling set by a decreasing M. In high fields, the H dependence of $e_N=\rho\alpha_{xy}^s \sim M(H)$ follows that of $M(H)$ since ρ becomes nearly H independent once H exceeds $\sim 2\ H_m$ (in LSCO and YBCO; in Bi 2201 and Bi 2212, the saturation in ρ is much more gradual).

A similar hill profile is observed in the Ettingshausen signal in the superconductor PbIn (Fig. 10).[48] The signal rises steeply to a maximum when the vortex lattice is depinned. As H approaches H_{c2}, the signal decreases to zero $\sim(H_{c2}-H)$. The small "tail" above H_{c2} is due to amplitude fluctuations. As discussed in Sec. II, the Ettingshausen signal $\sim\tilde{\alpha}_{xy}^s$ has the same H dependence as α_{xy}^s.

By contrast, the qp signal e_N^n is nominally linear in H with a small H^3 correction observable only in high fields ($>$20T) at low T ($<$10 K). The short qp mean free path ℓ in hole-doped cuprates ($\ell \sim 80$ Å at 80 K) precludes any possibility of observing a hill-type profile in e_N^n even in fields 20–40 T.

Figure 11 shows Nernst curves measured in OP Bi 2201 in H up to 45 T. The curves taken below T_c (28 K) all display the tilted-hill profile. As H is increased above H_m, e_N rises steeply to a prominent maximum and then falls more slowly in high fields with a slope that is only weakly H dependent. Significantly, when we exceed T_c, the curves retain the same hill profile (see curves at 30–45 K). In fact, the curves up to 65 K show the same nominal profile except that the maximum is quite broad. However, above $\sim$50 K, the negative qp term e_N^n grows in significance and pulls e_N towards negative values at large H.

Similar results are also seen at other dopings. In Fig. 12(a) we show Nernst results on OV Bi 2201 (y_{La}=0.2) with T_c=22 K. Even at T=40 K or $\sim 2T_c$, the curve retains the characteristic hill profile of the vortex signal. In underdoped

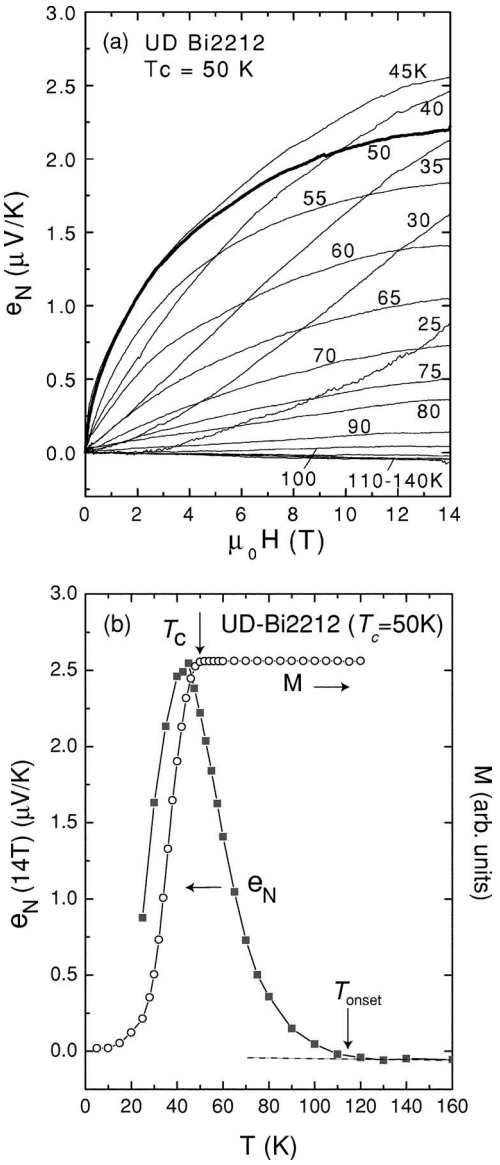

FIG. 9. (a) Curves of e_N vs H in UD Bi 2212 from 25 to 140 K. The bold curve is taken at T_c=50 K. The curves remain strongly nonlinear up to 70 K. (b) Comparison of the T dependence of e_N measured at 14 T and the Meissner curve (M at 10 Oe) in UD Bi 2212. The vortex signal deviates from the qp background at $T_{onset}\sim$118 K.

Bi 2201 (y_{La}=0.7) shown in Fig. 12(b), the effect is even more dramatic. The curves of e_N measured above T_c (=12 K) continue to show a vortex profile up to our highest temperature 30 K. The extension of the tilted-hill profile to T high above T_c implies that the same mechanism generating e_N below T_c—vortex flow—must be operating above T_c.

A graphic way to represent the continuity between the Nernst region above T_c and the vortex-liquid state below T_c is the contour plot in the T-H plane.[21] In Fig. 13, the gray scale represents regions with successively higher values of e_N in Bi 2201 (y_{La}=0.4). The black area (e_N=0) is the vortex solid phase below $H_m(T)$. If we increase H at fixed $T<T_c$ (=28 K), e_N climbs rapidly just above H_m and attains

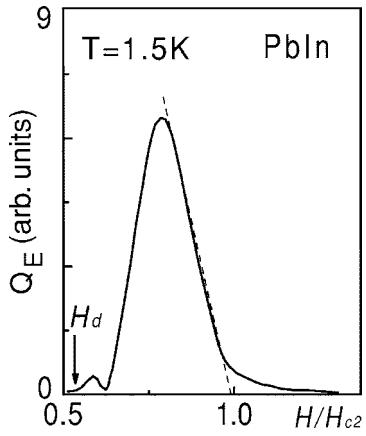

FIG. 10. The Ettingshausen signal $\mathcal{Q}_E$ vs H in the type-II superconductor PbIn (adapted from Ref. 48). The H dependence of $\mathcal{Q}_E$ has the characteristic peak profile of the vortex response. The dashed line locates H_{c2} determined by ρ vs H. Above H_{c2}, the signal displays a weak fluctuation tail.

a maximum (lightest shade), before dropping gradually towards zero at H_{c2} (solid squares are $H_{c2}(T)$ values discussed in the next section). All the preceding figures displaying curves of e_N vs H are vertical cuts in the T-H plane. The maxima in the e_N-H curves define the ridge field $H_{ridge}(T)$ (dashed curve in Fig. 13). As the pair condensate remains very large above H_{ridge}, it clearly lies far below the depairing field H_{c2}. We discuss H_{ridge} in relation to ρ in Sec. VIII.

The contour plot provides a global view of the tilted-hill profiles shown in Fig. 11. The strong curvature of the contour lines at high T implies that the hill profile is also observed above T_c, as noted above. From the contour plot, it is clear that the vortex liquid state just above H_m smoothly

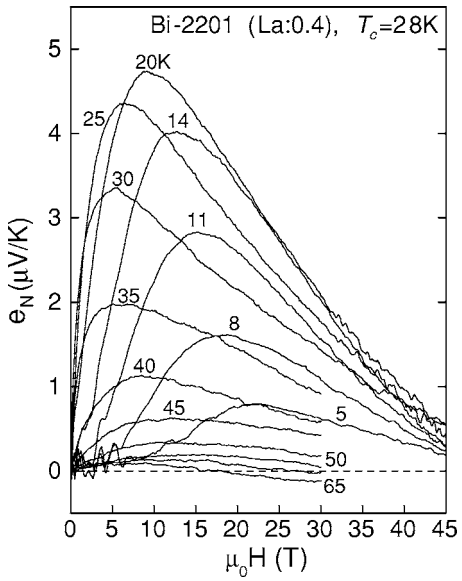

FIG. 11. Curves of e_N vs H in OP $Bi_2Sr_{2-y}La_yCuO_6$ (with La content y_{La}=0.4, T_c=28 K) measured to intense fields (45 T below 35 K and 32 T above 35 K). The depairing field H_{c2} is determined by extrapolation of e_N to zero. Above 60 K, the weak negative qp contribution becomes apparent.

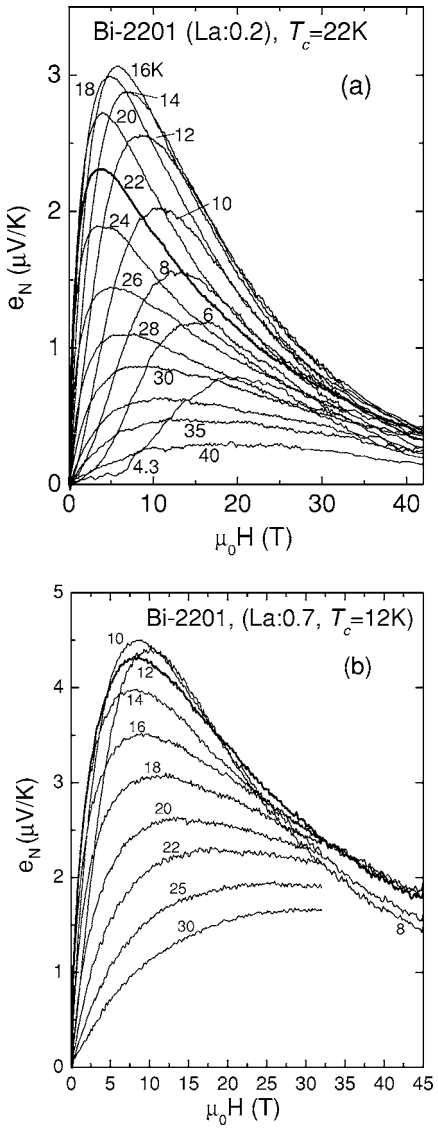

FIG. 12. (a) Curves of e_N vs H in OV $Bi_2Sr_{2-y}La_yCuO_6$ (y_{La}=0.2, T_c=22 K) measured to intense fields from 4.3 to 40 K. At all T, the curves appear to extrapolate to zero at the same nominal field scale (42–45 T). (b) Curves of e_N vs H in UD $Bi_2Sr_{2-y}La_yCuO_6$ (y_{La}=0.7, T_c=12 K) measured to 45 (32) T for temperatures below (above) 12 K.

extends into the Nernst region above T_c. There is no phase boundary discernible between the two regions; the vortex liquid state below T_c spreads continuously to temperatures above T_c. Overall, the magnitude of $e_N(T,H)$ changes very smoothly over the whole T-H plane. The only indication of T_c is the approach of the shallow contour minima towards 28 K as $H\rightarrow 0$. We refer the reader to Refs. 21, 23, and 24 for contour plots of LSCO and YBCO. The contrasting contour plot in NCCO is discussed below (Sec. X).

VII. UPPER CRITICAL FIELD

In the hole-doped cuprates, the upper critical field (or depairing field) H_{c2} is a rather poorly established quantity compared with the other parameters of the superconducting state. On the one hand, flux-flow resistivity experiments have given a very low estimate of H_{c2} (Refs. 68 and 69) (ρ is discussed at the end of this section). On the other hand, it was widely believed that H_{c2} in the cuprates is an inherently *unmeasurable* quantity.

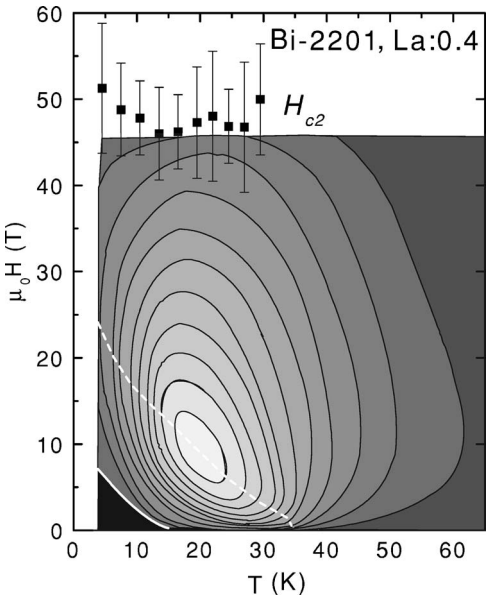

FIG. 13. Contour plot of $e_N(T,H)$ in OP Bi 2201 (y_{La}=0.4). The value of e_N is highest in the light-gray region and zero in black regions. The white curve terminating at 15 K is $H_m(T)$. The dashed curve is the ridge-line joining points of maxima of e_N vs H. Solid squares are values of H_{c2} estimated from extrapolation of the curves in Fig. 11. The plot emphasizes the smooth continuity of the vortex signal to temperatures high above T_c (28 K).

A powerful advantage of the Nernst experiment is that it provides a direct determination of H_{c2} that remains sensitive in intense magnetic fields. In type-II superconductors, as $H\rightarrow H_{c2}$ from below, the packing of vortex cores steadily reduces the volume fraction of the condensate in the interstitial "puddles" between cores. The coherence length ξ is related to the upper critical field by $H_{c2}=\phi_0/(2\pi\xi^2)$. For fields just below H_{c2}, the supercurrent is[70]

$$\mathbf{J}_s = -\frac{e\hbar}{m}\boldsymbol{\nabla}\times|\Psi|^2\hat{\mathbf{z}} \tag{11}$$

(with $\mathbf{H}||\hat{\mathbf{z}}$). The (diamagnetic) circulation of the supercurrent $\mathbf{J}_s$ around each of the interstitial condensate puddles generates a magnetization $\mathbf{M}$ that is greatly reduced from its value near H_{c1} and given by Abrikosov's expression

$$\mathbf{M} = -\frac{(H_{c2}-H)\hat{\mathbf{z}}}{\beta_A(2\kappa^2-1)}, \tag{12}$$

with $\beta_A\sim 1$ and $\kappa=\lambda/\xi$, where λ is the penetration length. Traditionally, the curve of M vs H has provided the most reliable method for finding H_{c2}.

However, in the cuprates, where $\kappa\sim 100$ and $H_{c2}\sim 50-150$ T, resolving the greatly suppressed M in high fields has been a formidable challenge. Recently, though,

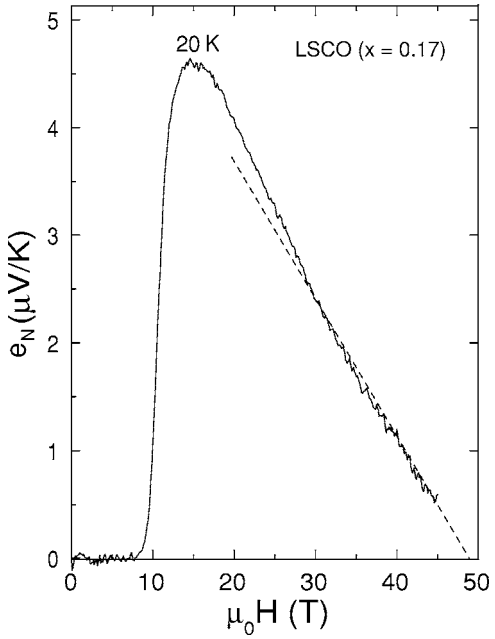

FIG. 14. The curve of e_N vs H measured at $T=20$ K in OP LSCO ($x=0.17$, $T_c=36$ K). The value of $H_{c2}\sim 50$ T is estimated by the dashed-line extrapolation of the high-field data to zero.

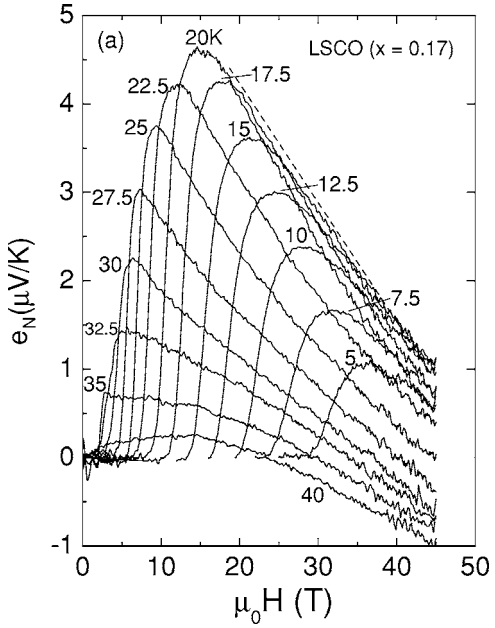

FIG. 15. The high-field Nernst curves in optimally doped LSCO ($x=0.17$) from 5 to 40 K. Below 20 K, all curves merge to the dashed line at high fields. As T rises above 20 K, the qp contribution increasingly "pulls" the curves of e_N to negative values in high fields. This effect is much less pronounced at lower T.

rapid progress is being made using high-field torque magnetometry (some of the new M vs H results are discussed in Sec. IX).

The Nernst experiment provides an alternative way to measure H_{c2}. As stressed in Sec. VI, the curve of e_N vs H has a characteristic peaked profile. On the high-field side, e_N is driven inexorably to zero in proportion to the magnetization [Eq. (12)]. This is clearly seen in the Ettingshausen curve in the low-T_c superconductor PbIn discussed in Sec. II (Fig. 10). The signal peaks near 0.8 H_{c2} and then decreases to zero as $(H_{c2}-H)$ (ignoring the high-field tail caused by amplitude fluctutations). The high-field end point of α_{xy}^s (or $\tilde{\alpha}_{xy}^s$) may be used to locate H_{c2}.

In most cuprates, the values of H_{c2} exceed the 45-T maximum available in current dc magnets. In analogy with the low-T_c case, we assume that linear extrapolation of the high-field Nernst signal to zero gives a reliable determination of the scale of H_{c2}. Adopting this assumption, we have broadly applied high-field Nernst experiments to estimate H_{c2} in several cuprate families.

First, we consider optimally doped LSCO ($x=0.17$, $T_c=36$ K). In Fig. 14, the extrapolation of e_N at 20 K gives $H_{c2}\sim 50$ T. Figure 15 displays e_N vs H in this sample at selected T. An interesting trend that is immediately apparent is that, in high fields, all the curves below 20 K merge to a common line (dashed line). With H_{c2} determined by linear extrapolation, we obtain the conclusion that H_{c2} is almost T independent from 5 K to 20 K. Unfortunately, in OP and OV LSCO, the qp negative background is moderately large above 20 K. As shown in Fig. 15, the H-linear qp term added to the diminishing vortex term "pulls" the observed e_N to negative values. This prevents H_{c2} from being readily estimated above 20 K in OP and OV LSCO. However, because α_{xy^n} is an entropy current, the qp term must decrease to zero as $T\rightarrow 0$ (this is shown for UD LSCO in Ref. 20). Hence it does not affect our estimate of H_{c2} at low T.

Determination of H_{c2} is most reliably carried out in single-layer Bi 2201 where the qp contribution is very small and H_{c2} values slightly more accessible. Figure 16 displays curves of e_N in optimally doped Bi 2201 ($y_{La}=0.4$). We show the linear extrapolations as dashed lines. Again, we see that

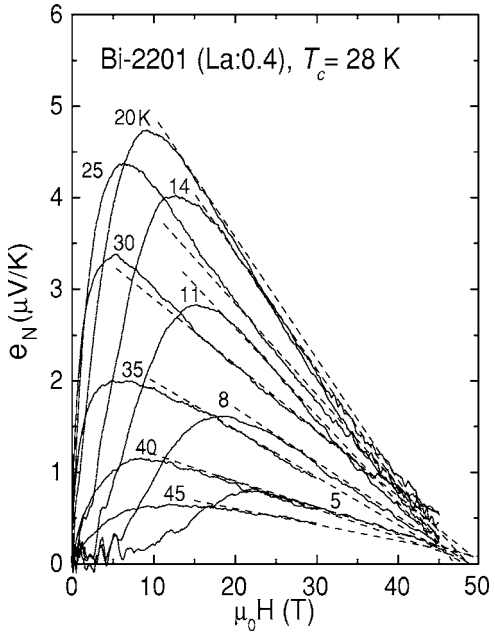

FIG. 16. Extrapolation of the curves of e_N (dashed lines) to determine H_{c2} values in OP Bi 2201 ($y_{La}=0.4$). The estimated values of H_{c2} are virtually T independent.

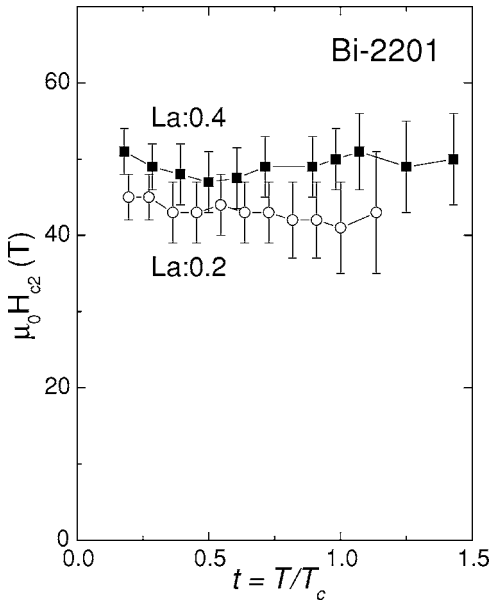

FIG. 17. Plot of H_{c2} versus the reduced temperature $t=T/T_c$ in OP and OV Bi 2201 (with $y_{La}=0.4$ and 0.2, respectively). At each T, H_{c2} is estimated as in Fig. 16.

the curves all extrapolate to zero at nearly the same H. This implies a T-independent H_{c2} value of 48 ± 4 T for temperatures from 5 to 45 K. We remark that, quite independent of the extrapolations, the convergent behavior of the measured curves already reveals this surprising result. This trend is also seen at other dopings. The Nernst traces in overdoped Bi 2201 ($y_{La}=0.2$) also exhibit this convergence (Fig. 12).

Curves of H_{c2} vs T in optimally doped and overdoped Bi 2201 are displayed in Fig. 17. Within the uncertainty of the data, the H_{c2} values in both samples are T independent from 4 K to well above T_c. This behavior is in sharp contrast with low-T_c type-II superconductors where H_{c2} decreases linearly as $H_{c2}\sim(T_c-T)$ near T_c. The data show that the H_{c2} values continue nearly unchanged for a significant interval above T_c.

This anomalous result is closely related to findings from ARPES (Refs. 64 and 71) that the gap amplitude Δ_0 in Bi 2212 is nearly T independent below T_c, and varies only weakly above T_c. Tunneling experiments on Bi 2201 have also shown that the gap does not close at T_c but remains finite above T_c.[73] We may relate Δ_0 to the Pippard length ξ_P by

$$\xi_P = \frac{\hbar v_F}{a\Delta_0}, \tag{13}$$

where $a\sim1.5$ for a d-wave gap (compared with π for an s-wave gap) and v_F the Fermi velocity. Assuming that $\xi\sim\xi_P$ in our samples, we have $H_{c2}\sim\Delta_0^2$. Hence the constancy of the gap amplitude across T_c implies our finding that H_{c2} is constant across T_c. In Ref. 22 the doping dependence of ξ_P inferred from ARPES is shown to be quantitatively similar to that of ξ obtained from the Nernst experiment. Finally, recent measurements of M vs H to 33 T have confirmed this anomalous constancy of H_{c2} across T_c in UD and OP Bi 2212 (Sec. IX).

As reported in Ref. 72, the gap amplitudes Δ_0 in a slightly UD and an OV Bi 2212 are nominally T independent from low T to well above T_c. It is instructive to compare these curves with our inferred H_{c2} vs T plot in Fig. 17. Both experiments imply that, in the cuprates, H_{c2} is nearly unchanged from low T to above T_c.

As mentioned, the constancy of H_{c2} across T_c is strikingly inconsistent with the mean-field BCS scenario in which $|\Psi|^2$ vanishes at T_c. By contrast, it supports strongly the scenario that the collapse of the Meissner state at T_c is caused by the loss of long-range phase coherence, with $|\Psi|$ remaining finite above T_c. The loss of phase coherence arises from the spontaneous generation of vortices and the resultant rapid phase slippage caused by their motion. The constancy of H_{c2} up to T_c implies that it actually goes to zero only at a much higher temperature (the mean-field transition $T_c^{MF}\gg T_c$). In the 2D KT transition, Doniach and Huberman[13] have noted that H_{c2} (or the depairing field) must remain at a high value across the KT transition temperature T_{KT}. In summary, the anomalous behavior of H_{c2} in the hole-doped cuprates strongly supports our vortex interpretation of e_N.

The doping dependence of H_{c2} was initially investigated from the slightly UD regime to the OV regime. In Ref. 22, it was found that H_{c2} decreases systematically from slightly UD to OP to OV samples in Bi 2212, Bi 2201, and LSCO. The trend agrees with that of Δ_0 measured by ARPES in Bi 2212 by Harris *et al.*[71] and Ding *et al.*[72] Further, the values of ξ inferred from H_{c2} vs x (Ref. 22) are consistent with ξ_P obtained from Δ_0 and with the vortex core size observed by STM.[74]

We have now extended these H_{c2} estimates over the whole doping range in LSCO in five crystals with $x=0.05$, 0.07, 0.12, 0.17, and 0.20. The values of H_{c2} determined at our lowest T (4.2 K)—which we identify as $H_{c2}(0)$—are plotted as solid squares in Fig. 18. As shown, the x dependence of $H_{c2}(0)$ is nominally similar to that of T_{onset} (open circles). As x increases from 0.03, $H_{c2}(0)$ rises very steeply to peak near 0.10 and then decreases more gradually towards 0 as $x\rightarrow0.26$. (The values for $x>0.10$ are in agreement with the estimates reported in Ref. 22, but the steep fall on the low-x side was not investigated in that study.)

Resistivity. In low-T_c type-II superconductors, the flux-flow resistivity ρ provided a convenient means to determine H_{c2}. If the applied current I is high enough to depin the vortex lattice, ρ increases linearly as $B\phi_0/\eta=(H/H_{c2})\rho_N$ to reach the normal-state value ρ_N at H_{c2} (the Bardeen-Stephen law[19]). Conveniently, H_{c2} is often flagged by a sharp notch minimum in ρ (the peak effect). The Bardeen-Stephen law is rarely—if ever—observed in cuprates. Just above the melting field $H_m(T)$, ρ rises very rapidly to saturate at a value close to that of the pretransition ρ suitably extrapolated below T_c. Two examples of ρ-H profiles are shown in Fig. 19 in OV LSCO ($x=0.20$). Previously, attempts were made to identify the "knee" feature corresponding to this saturation with "H_{c2}."[68,69] The inferred curve of H_{c2} vs T invariably displayed the wrong curvature, together with anomalously low depairing fields (0.01–0.1 T) near T_c. They are strik-

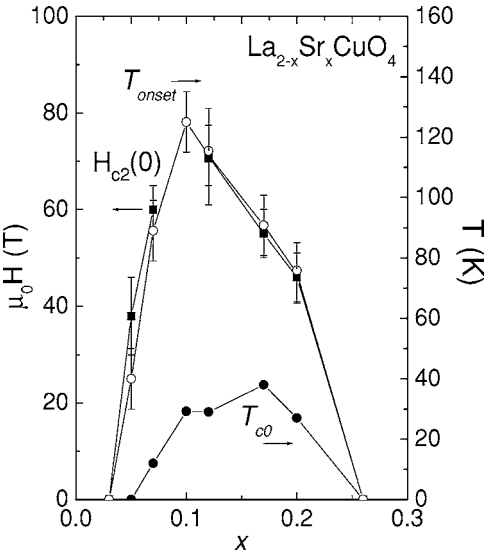

FIG. 18. Variation of the low-T upper critical field $H_{c2}(0)$ estimated at 4.2 K versus x in LSCO (solid squares). The values are estimated by extrapolation of e_N^s to zero from measurements in H to 45 T. For comparison, we also plot T_{onset} (open circles) and T_c (solid circles). Lines are guides to the eye.

ingly incompatible with the H_{c2} values obtained from the Nernst results.

The field profiles of ρ and e_N at 22 K are compared in Fig. 19. As mentioned, the knee feature in ρ occurs near $H_{ridge} \sim 5$ T. However, the vortex signal remains quite large above the knee, eventually decreasing to zero at the much higher $H \sim 48$ T. At 12 K, the knee feature in ρ is much broader, but it occurs at ~ 20 T, still considerably below

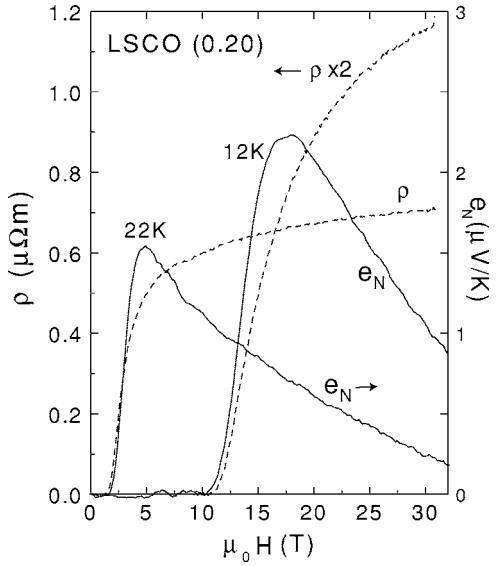

FIG. 19. Comparison of the field profiles of the flux-flow resistivity ρ and the Nernst signal e_N measured on the same sample, an overdoped crystal of LSCO (x=0.20) at T=22 and 12 K. Above H_m, ρ quickly approaches saturation to the resistivity value extrapolated from above T_c (this occurs near H_{ridge} defined by the peak in e_N). However, e_N decreases to zero at the depairing field H_{c2} which lies much higher ($H_{c2} \sim 45$ T).

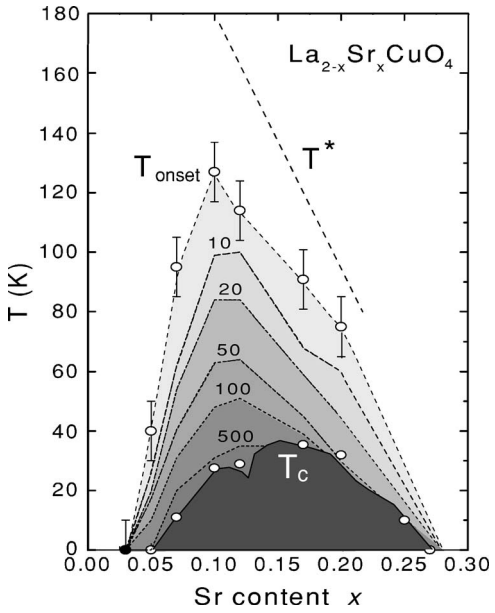

FIG. 20. The phase diagram of LSCO showing the Nernst region between T_c and T_{onset} (numbers on the contour curves indicate the value of the Nernst coefficient ν in nV/KT). The curve of T_{onset} vs x has end points at x=0.03 and x=0.26 and peaks conspicuously near 0.10. The dashed line is T^* estimated from heat-capacity measurements.

48 T. The comparison emphasizes the fallacy of identifying the saturation of ρ with a depairing field scale. The condensate amplitude remains robust up to considerably higher fields. We argue that the knee feature instead reflects the shrinking with increasing field of the length scale over which phase *stiffness* holds. This loss occurs in the field interval between H_m and the H_{ridge} curve (dashed line in Fig. 13). In Bi-based cuprates this loss is quite gradual, whereas in OP-OV YBCO and LSCO it is abrupt (Figs. 3 and 14, respectively). Further, above H_m, the dissipation climbs much more rapidly than prescribed by the Bardeen-Stephen law. This rapid increase implies a very weak damping viscosity η and is known as the fast-vortex problem (Sec. XI).

VIII. PHASE DIAGRAM, ONSET TEMPERATURE, AND MAGNITUDE

In the phase diagram of the cuprates, superconductivity occupies a dome-shaped region defined by the curve of T_c vs x. The pseudogap temperature T^* decreases monotonically from the scale 300–350 K to terminate at the end point x_p (the Nernst experiments along with many experiments indicate that $x_p \sim 0.26$, but other groups[75] favor x_p=0.19). As reported previously,[20,24] in the phase diagram of LSCO, the onset temperature of the Nernst signal T_{onset} falls between T^* and T_c. As x increases from 0.03, T_{onset} rises steeply to a maximum value of 130 K at 0.10 and then falls more gradually to a value near zero at ~ 0.27 (Fig. 20).

We turn next to T_{onset} in bilayer Bi 2212. In Fig. 21, we display the variation of T_{onset} in the five crystals investigated to date. The hole density x is estimated from the

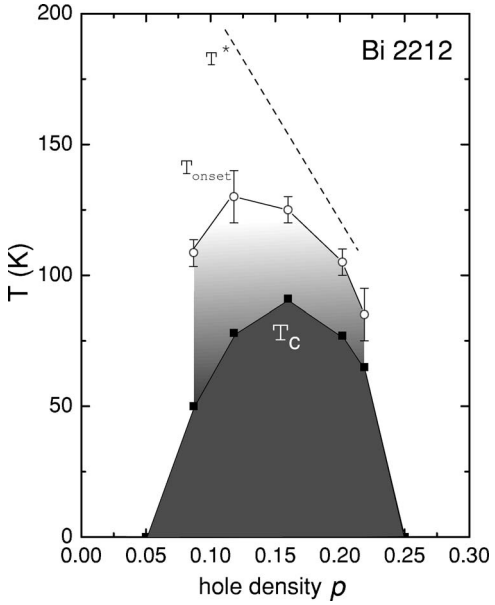

FIG. 21. The phase diagram of Bi 2212 showing the Nernst region between T_{onset} and T_c (based on Nernst measurements on five crystals). As in LSCO (Fig. 20), the Nernst region does not extend to the pseudogap temperature T^* on the OP and OV sides. In the UD regime, T_{onset} shows a decreasing trend as x decreases below 0.15.

empirical formula $T_c(x)=T_{c,max}[1-82.6(x-0.16)^2]$, with $T_{c,max}=91$ K.[76] The curve of T_{onset} shares key features with that found in LSCO. As in LSCO, the superconducting dome in Bi 2212 is nested inside the curve of T_{onset} vs x which lies under the curve of T^*. Whereas T^* appears to continue to increase as x falls below 0.10, T_{onset} deviates downwards in qualitative similarity with LSCO. The interval between T_{onset} and T_c becomes systematically narrower towards the OV side, but it remains quite broad on the UD side. Interestingly, the maximum value of T_{onset} ($\sim$130 K) is close to the maximum in LSCO, despite the large difference in maximum T_c in the two families. The maximum value in YBCO is $\sim$130 K as well. However, in the Hg-based cuprates, evidence from torque magnetometry suggests that T_{onset} lies higher.[77]

In the phase diagrams in Figs. 20 and 21, the nesting of the T_c dome within the curve of T_{onset} underscores once more the continuity of the region in which the vortex-Nernst signal is observed with the region under the superconducting dome. The high-temperature e_N associated with vortices is observed only inside the superconducting dome. Once we move outside (either on the UD or OV side), e_N becomes very small. In LSCO with $x=0.03$ and 0.26, the tilted-hill profile characteristic of vortex flow is completely absent. Instead, the observed e_N is small and H linear to fields as high as 33 T, which is characteristic of the qp current.

On the UD side, the rapid vanishing of the vortex-Nernst signal for samples with $x=0.03$, 0.05, and 0.07 has already been analyzed in detail in Ref. 20. Because the vortex signal is rapidly decreasing relative to the qp signal, it is necessary to measure the Hall angle and thermopower to separate out the two contributions to the off-diagonal Peltier term $\alpha_{xy}=\alpha_{xy}^s+\alpha_{xy}^n$.[20]

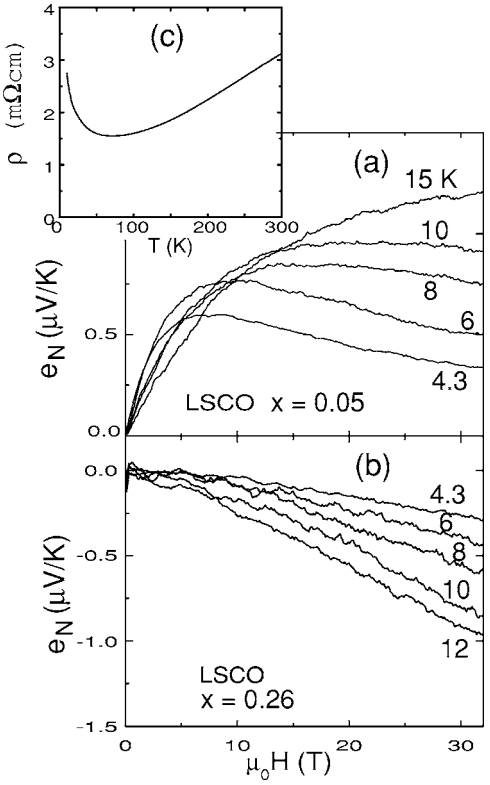

FIG. 22. Comparison of the Nernst curves in severely UD LSCO [$x=0.05$, panel (a)] and heavily OV LSCO [$x=0.26$, panel (b)]. In both samples, $T_c<2$ K and the observed Nernst signal is weak. However, in the UD sample, e_N retains the "tilted-hill" profile characteristic of vortices, whereas e_N in the OV sample shows only the negative, H-linear qp contribution. The resistivity profile ρ vs T of the UD sample is shown in panel (c).

It is interesting to compare the Nernst signals at the two extremes of the T_c dome. Figure 22 shows e_N measured in UD LSCO [$x=0.05$, panel (a)] and in OV LSCO [$x=0.26$, panel (b)]. In both samples, $T_c<2$ K. As shown in Fig. 23, the Nernst signals in these two samples are about 10 times smaller than the largest signals observed in superconducting LSCO. However, these two samples exhibit strongly contrasting Nernst behaviors. In the UD sample, e_N is strongly nonlinear in H, displaying the "tilted-hill" profile characteristic of the vortex signal, whereas e_N in the OV sample shows only the negative, H-linear contribution from quasiparticles. In the UD sample, phase disordering caused by vortex motion destroys superconductivity (in $H=0$). However, the pair condensate is robust to intense fields (the Nernst curves show that H_{c2} is larger than 40 T). By contrast, in the OV sample, superconductivity above 2 K is absent because the pair condensate is absent altogether. Moreover, the resistivity profile in the UD sample shows an insulating trend below $\sim$80 K [panel (c)], whereas the OV sample remains metallic down to 2 K. These differences reflect the presence of the pseudogap on the UD extreme of the T_c dome and its absence on the OV extreme.

The doping dependence of the magnitude of the Nernst signal also reveals an interesting pattern that complements the previous point (that the vortex e_N is confined to within

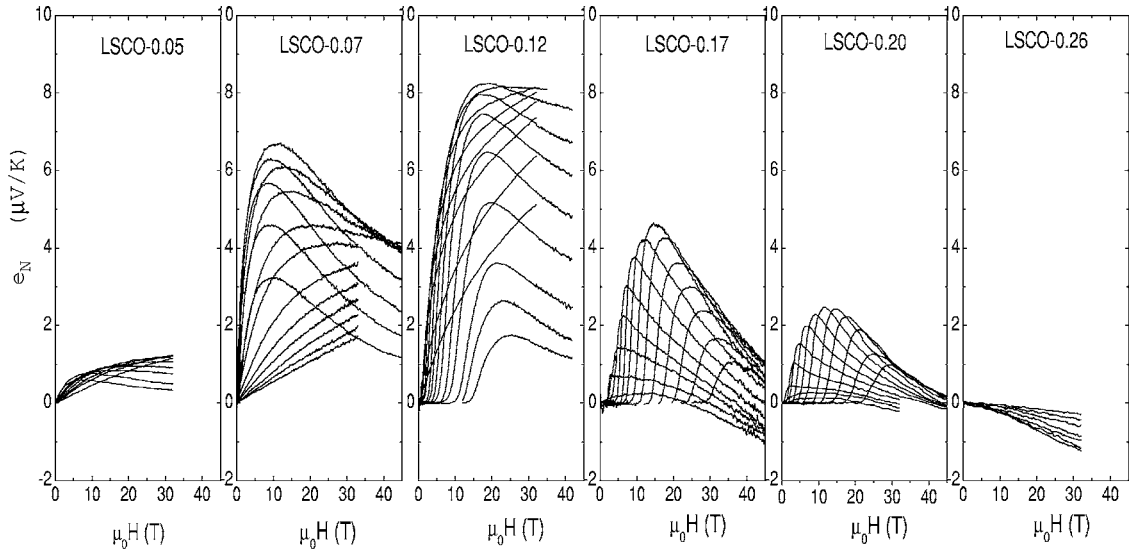

FIG. 23. Comparison of curves of e_N vs H in LSCO samples with (from left panel to right) $x=0.05$, 0.07, 0.12, 0.17, 0.20, and 0.26. The same x and y scales are used in all panels. In each panel, the envelope curve provides a measure of the overall magnitude of the vortex signal.

the dome). Figure 23 displays the high-field Nernst results of six LSCO samples at various T. The hole density x and T_c values of these samples are 0.05 (0 K), 0.07 (11 K), 0.12 (29 K), 0.17 (36 K), 0.20 (28 K), and 0.26 (0 K), respectively (the x and y scales are the same in all panels).

In each sample, the Nernst curves are nested within an envelope which has a peak value. In the doping range $0.12 \leqslant x \leqslant 0.20$, the envelope peaks at $\sim \frac{1}{2} T_c$, whereas in very UD samples ($x=0.05$ and 0.07), it peaks above T_c. As x increases, the peak value rises to the value $e_N^{max} \sim 8.3\ \mu$V/K near 0.12 and falls rapidly as x reaches 0.26. The variation of the peak value e_N^{max} with x is summarized in Fig. 24, together with the curves of T_c and T_{onset} in the same samples.

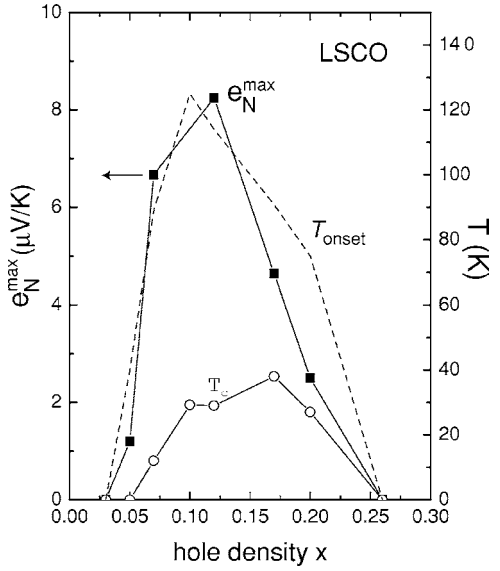

FIG. 24. The variation with x of the maximum vortex-Nernst signal e_N^{max} (solid symbols), T_c (open circles), and T_{onset} (dashed line) in LSCO. Solid lines are guides to the eye.

The plots in Figs. 23 and 24 show that the large Nernst signal observed in LSCO crystals are intimately related to the T_c dome. When we go beyond the dome on either side, the peak value e_N^{max} falls rapidly towards zero. Examination of the panels in Fig. 23 shows that, in each sample, e_N^{max} also dictates the overall scale of the Nernst signal both above and below T_c. Hence we deduce that large Nernst signal derives from the superconducting pairs. In the UD limit where a large pair density cannot be sustained, or in the OV limit when pairing is absent, the vortex-Nernst signal vanishes, leaving only the usual qp term. The tight correlation between the overall amplitude of the signal and the T_c dome plays an important role in refuting theories that interpret the large Nernst signal as caused by quasiparticles in some exotic state that abuts the superconducting dome (we discuss this in Sec. XI).

IX. ENHANCED DIAMAGNETISM ABOVE T_c

The evidence for vortices above T_c described in the preceding sections would seem to be sufficiently compelling. However, for reasons already listed (Sec. III), it was desirable to seek evidence from nontransport experiments. In searching for other probes of phase fluctuations, we reasoned that, even if long-range phase coherence is destroyed by vortex motion, the large supercurrent $\mathbf{J}_s$ circulating around the condensate puddles [see Eq. (11)] should persist on length scales slightly larger than the average vortex spacing $a_B \sim (\phi_0/B)^{1/2}$. Hence, above T_c, the magnetization must retain a weak diamagnetic term analogous to Eq. (12). This diamagnetism should be non-Gaussian and *survive* to 33 T and beyond if it is to be related at all to e_N. Although in previous studies of "fluctuation diamagnetism" in cuprates, a few reports found[78,79] anomalous features that lie outside the purview of conventional Gaussian theory, the majority reported satisfactory agreement (and even a good fit[80]) with Gaussian theory. Naughton has drawn our attention to his

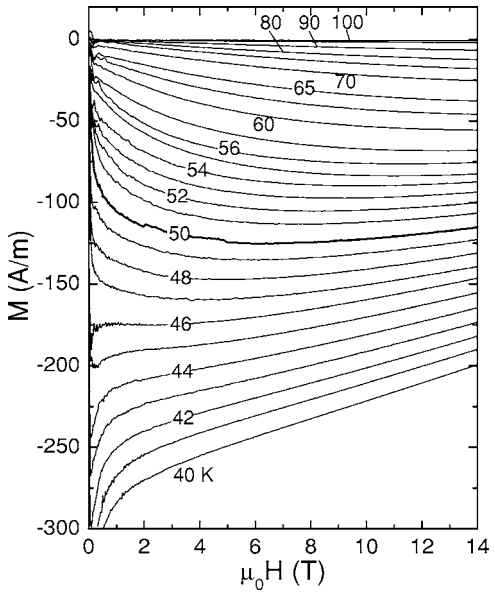

FIG. 25. Magnetization curves M vs H in UD Bi 2212 (T_c=50 K) at temperatures from 40 to 200 K. The magnetization is extracted as a strongly T-dependent diamagnetic contribution to the total torque signal in a Si cantilever (Ref. 81). The bold curve is taken at T_c=50 K. Even at 70 K, $M(H)$ displays nonlinearity in H.

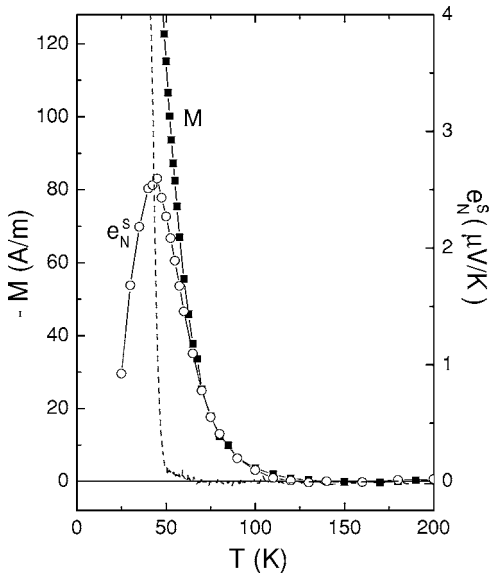

FIG. 26. The T dependence of e_N^s (open circles) and the diamagnetic signal $-M$ (solid squares) in UD Bi 2212. Both quantities were measured at 14 T in the same crystal (e_N^s is the vortex-Nernst signal obtained after subtracting the small negative qp contribution e_N^n from the total Nernst signal). The dashed line is the weak-field Meissner effect of this sample measured at H=10 Oe measured by SQUID.

report[77] of an unexplained diamagnetic signal in Hg 2212 that persists to 33 T and 200 K.

Because the diamagnetic component of **M** is strictly $||\hat{\mathbf{c}}$ in the phase-fluctuating regime above T_c ($\mathbf{J}_s$ is confined within the CuO_2 layers), torque magnetometry with **H** tilted slightly away from $\hat{\mathbf{c}}$ is ideally suited for resolving a very small M from the background torque signal (the background arises from the anisotropic spin susceptibility $\Delta\chi_p$).[81] In collaboration with Naughton, we have performed extensive measurements of M above T_c in several crystals of LSCO and Bi 2212 using a sensitive Si cantilever magnetometer.[53,81]

Here we briefly report results that are closely relevant to this paper (see Ref. 81 for details). Figure 25 displays M vs H curves of an underdoped Bi 2212 (T_c=50 K) obtained from torque magnetometry. The background term $\Delta\chi_p$ which is weakly T dependent has been subtracted. The diamagnetic signal starts to appear near 120 K and increases in magnitude over a broad 70-K interval above T_c. At T_c=50 K (bold curve), the diamagnetic signal attains the value of -120 A/m. At even lower T, the rapid growth of the Meissner effect becomes apparent at low field and the M-H curves resemble those in low-T_c type-II superconductors. The Nernst curves measured on this crystal was shown in Fig. 9.

The magnetization measurements on underdoped Bi 2212 are remarkably consistent with the Nernst results. In Fig. 26, the temperature dependence of the vortex-Nernst signal e_N^s and the diamagnetic signal measured at H=14 T are plotted together. Both deviate from the flat normal background at $T\sim 120$ K, indicating the onset of strong fluctuations well above the T_c defined by the sharp Meissner transition (dashed line). The two signals track each other closely over a broad interval of T from 120 K down to $\sim$65 K below which e_N^s attains a peak before sharply falling to zero (as the vortex-solid phase is approached). Scaling between e_N^s and M is also observed in OP and OV Bi 2212.[81]

The scaling observed confirms that the vortex-Nernst effect is accompanied by a weak diamagnetic response within the CuO_2 layers, which we identify with local supercurrents within the interstitial puddles between mobile vortices (Sec. VII). The scaling observed above T_c suggests that the linear relation between α_{xy}^s and M extends beyond the restricted regime of Eq. (5) found by Caroli and Maki, and may have rather broad generality. We also remark that even at such high T, M is robust in field, surviving to above 33 T (Ref. 81) (the curves in Fig. 25 are displayed to 14 T). As noted in Ref. 81, the robustness of M here distinguishes it from "fluctuation" diamagnetism arising from amplitude fluctuation familiar in low-T_c superconductors.[56] We emphasize the importance of the magnetization results in providing thermodynamic evidence that confirms the transport Nernst results and refer the reader to Ref. 81.

X. ELECTRON-DOPED CUPRATE

The electron-doped cuprate $Nd_{2-x}Ce_xCuO_{4-y}$ (NCCO) provides an interesting counter example to the hole-doped cuprates. Although NCCO shares the layered structure comprised of CuO_2 planes, its phase diagram differs from that of the hole-doped cuprates. The 3D antiferromagnetic (AF) state extends up to $x\sim 0.15$, and the superconducting region is confined to a narrow doping range (0.15–0.17) abutting the AF state. A pseudogap phase has not been detected above T_c (below T_c a residual gap is detected if superconductivity is completely suppressed by a field; whether this is simply the AF gap is still an open question).

Figure 27 shows curves of e_N vs H in optimally doped NCCO (x=0.15 and T_c=24.5 K) between 5 and 30 K.[22,83] In

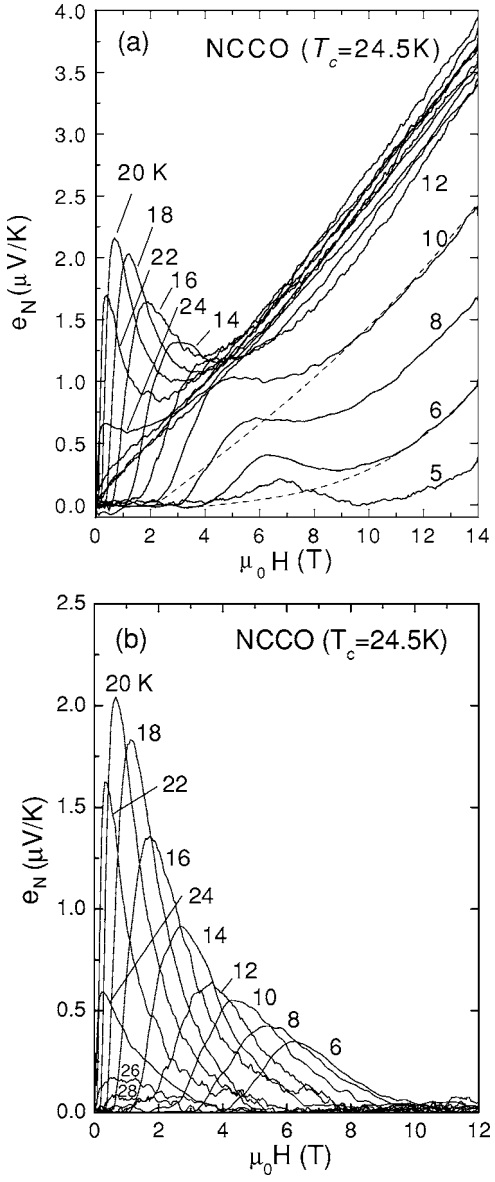

FIG. 27. (a) Curves of the observed Nernst signal e_N vs H in OP NCCO (x=0.15 and T_c=24.5 K) at temperatures 5 K to 30 K. The dashed lines are fits of the high-field segments to a qp term of the form $e_N^n(T,H)=c_1H+c_3H^3$. (b) The vortex-Nernst signal e_N^s extracted from panel (a) by subtracting $e_N^n(T,H)$ from the observed signal. The contour plot of this vortex signal is displayed in Fig. 28.

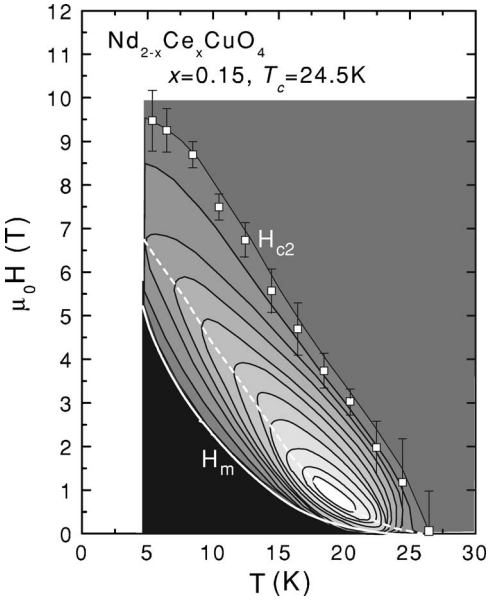

FIG. 28. The contour plot of the vortex-Nernst signal $e_N^s(T,H)$ in NCCO (x=0.15, T_c=24.5 K). The magnitude of e_N^s is highest in the light-gray region and zero in the black region below the melting-field curve $H_m(T)$ (white curve). The dashed curve is the ridge joining the maxima of the curves of e_N^s vs H. The upper critical field values H_{c2} estimated from where $e_N^s \to 0$ are shown as white symbols. The absence of a pseudogap correlates with the vanishing of the vortex-Nernst signal at T_c and the termination of the H_{c2} curve at T_c (contrast with Fig. 13 for Bi 2201).

this cuprate, the qp contribution to the Nernst signal is large. From early Hall-effect experiments[84,85] as well as ARPES, it is known that both electronlike and holelike bands contribute to the qp current. The presence of both bands leads to a change in sign of the normal-state Hall coefficient R_H in OP crystals.[84,85] As given in Eq. (6), the qp Nernst signal is the difference of two terms $\rho^n\alpha_{xy}^n$ and $\rho_{xy}^n\alpha^n$.[20] For a one-band system, cancellation between the two terms (dubbed[20] Sondheimer cancellation) greatly reduces e_N^n. However, if both holes and electrons are present, this cancellation is suppressed and e_N^n becomes enhanced. A clear example was recently demonstrated by Behnia's group in $NbSe_2$.[82]

A similar suppression of the cancellation exists in NCCO.[22,83] At 30 K, the qp Nernst coefficient $\nu^n \sim 0.26\ \mu$V/KT, which is ~10 times larger than that in OP and OV LSCO (and ~50 times larger than in Bi 2201 and Bi 2212). The observed Nernst signal is the sum of the vortex and qp terms [Eq. (7)]. In sharp contrast with results in hole-doped cuprates, the qp term actually dominates the Nernst signal at 6 K, far below T_c. Nevertheless, as evident in Fig. 27(a), the vortex term retains its characteristic tilted-hill profile which is easily distinguished from the monotonic qp term. By fitting the latter to the form $e_N^n=c_1H+c_3H^3$, with c_i as fit parameters at each T (dashed curves), we have extracted $e_N^s(T,H)$, which are displayed in Fig. 27(b).

The field profiles of the vortex signal are remarkably similar to those in OP Bi 2201 except that the depairing field scale is much lower here ($H_{c2} \sim 10$ T compared with ~50 T). The Nernst curves in Fig. 27(b) are also nested within an envelope curve that peaks sharply at 20 K.

However, there is an interesting difference above T_c. As $T \to T_c$=24.5 K from below, the individual hill profiles become narrower in field while the peak value decreases. The decrease in the peak value of e_N^s is so rapid that at 28 K, the vortex contribution falls below our resolution. The convergence to zero at T_c of the amplitude is similar to the behavior of e_N observed in low-T_c superconductors,[46] but contrasts sharply with that in the UD hole-doped cuprates.

The narrowing of the hill profiles also implies that $H_{c2}(T)$ decreases rapidly with increasing T. In Fig. 28 we plot as open squares H_{c2} determined as the field at which $e_N^s \to 0$ at each T. We find that it goes to zero linearly as $H_{c2} \sim (1-t)$ with the reduced temperature $t=T/T_c$. Again, this is similar

to $H_{c2}(T)$ in BCS theory. As discussed at length in Sec. VII, H_{c2} and e_N^s remain at very large values in all hole-doped cuprates as we cross T_c.

Figure 28 also shows the contours of the *vortex* signal e_N^s in NCCO. The contrast with the contour plot of Bi 2201 (Fig. 13) is instructive. Instead of spreading outwards to temperatures high above T_c, the regions of finite e_N^s here are confined to the vortex-liquid state between $H_{c2}(T)$ and $H_m(T)$, with the long axes of the contour ellipses roughly parallel to H_{c2}. Above $H_{c2}(T)$, e_N^s cannot be resolved. We determined the melting field $H_m(T)$ (solid white curve) as the line at which e_N^s first becomes detectable. The vortex-liquid state occupies a large fraction of the phase below the H_{c2} curve. Aside from this unusual feature, the phase diagram of NCCO is similar to that in a conventional low-T_c superconductor.

The Nernst results in NCCO are valuable in two aspects. The modest depairing scale ($H_{c2} \leqslant 10$ T) allows the full hill profile of e_N^s to be easily distinguished even though it is riding atop a larger qp term. The juxtaposition shows unequivocally that there exist two very different contributions to the total Nernst signal of cuprates, each with its distinct field profile. The close similarity of the profile of e_N^s to that of e_N in Bi 2201 provides evidence that our procedure for extracting H_{c2} in the latter is sound.

More significantly, the comparison reinforces the point that the persistence of e_N^s and H_{c2} above T_c in the hole-doped cuprates is closely tied to the pseudogap phenomenon. In NCCO where the pseudogap is absent (above T_c), the vortex Nernst signal is also absent. Moreover, the curve of H_{c2} terminates at T_c. The comparison shows that the high-temperature Nernst phase is not generic to any highly anisotropic layered superconductor with a modest carrier density (the resistivity anisotropy in NCCO is comparable to that in LSCO and UD YBCO). It is inherently related to the physics of the pseudogap state in hole-doped cuprates.

XI. DISCUSSION

States above and below T_{onset}. In the cuprate phase diagram, the Nernst region represents an extended area in which vorticity—hence charge pairing—survives above the curve of T_c vs x. In the hole-doped cuprates Bi 2201, Bi 2212, Bi 2223, LSCO, and YBCO, the Nernst results establish that T_c is primarily dictated by the loss of phase coherence due to spontaneous vortex-antivortex unbinding in $H=0$. In the Nernst region just above the T_c curve, the phase $\theta(\mathbf{r})$ is strongly disordered by rapidly diffusing vortices and antivortices, whereas closer to the curve of T_{onset}, fluctuations in the amplitude become equally important. It is important to note, however, that, in each cuprate family, the Nernst region does not extend all the way to the pseudogap temperature T^*. As shown in Figs. 20 and 21, T_{onset} lies roughly between T_c and T^* for doping $x > 0.10$. In the very UD regime ($x < 0.1$), T_{onset} falls steeply as $x \to 0$, whereas T^* seems to continue to increase. Our data show that the Nernst region is nested within the pseudogap region. (The data do not seem to support the recent proposal[2] that the curves of T_{onset} and T^* actually cross near 0.19.)

This implies that, as we cool an UD sample from room temperature, the pseudogap state appears first at T^* but is seen only in experiments that couple to the spin degrees. Cooling below T_{onset} produces the signals e_N and M, which result from the existence of vortices and a diamagnetic response, both distinct signatures of short-range supercurrents. It seems that, in order for the high-T pseudogap state to coexist with dSC (d-wave superconductivity) over the broad interval $T_{onset} > T > T_c$, the two states must be intimately related and be distinguished by a subtle difference. The Nernst region is where the system smoothly evolves or fluctuates between the two states.

Several interesting theories incorporating this subtle change have been proposed. According to Anderson,[34] the uniform resonating-valence-bond (RVB) state is stable above T_{onset}, but the spin triad defined by $\hat{\Delta}$ and $\hat{\zeta}$ (the self-energies derived from the magnetic interaction term) fluctuates strongly relative to the electron charge triad. At T_{onset}, the two triads lock to produce a vortex-liquid state that is, however, phase disordered (phase coherence occurs at T_c). In the SU(2) formulation of RVB,[2,87] the quantization-axis vector $\hat{\mathbf{I}}(\vartheta, \varphi)$ of the slave-boson spinor

$$\begin{bmatrix} b_1 \\ b_2 \end{bmatrix}$$

distinguishes the staggered-flux pseudogap state ($\vartheta \simeq 0, \pi$) from dSC ($\vartheta = \pi/2$). Above T_{onset}, $\hat{\mathbf{I}}$ points mostly towards the poles, but in the Nernst region, $\hat{\mathbf{I}}$ fluctuates away from the poles, eventually coming to lie in the equatorial plane below T_c. In the striped model, the competing state involves quasi-1D dynamic stripes.[3] Vortex excitations are also fundamental to other recent theories of the pseudogap and charge-ordered states above the T_c dome.[28,29,31–33] We anticipate that detailed experiments on e_N and M in intense fields, in combination with STM experiments above T_c, should allow these theories to be tested.

Cheap and fast vortices. An important issue raised by these results is the energy cost of creating the vortices. In the limit $\kappa \gg 1$ in BCS theory, the energy of a vortex line of length d arises chiefly from the superfluid kinetic energy and is given by[70] $E_V = \phi_0^2 d/(4\pi\mu_0\lambda^2)\ln\kappa = \pi K_s \ln\kappa$. Here, it is important to add to this the core energy E_c. The total energy E_{pc} of a vortex pancake is then[2,30]

$$E_{pc} = E_c + 2\pi K_s \ln L/\xi. \tag{14}$$

As $T \to T_c$ from below, the superfluid term in K_s vanishes. However, E_c does not in the phase-disordering scenario. In BCS theory, E_c is the loss of condensation energy inside an area ξ^2—viz, $E_c \sim \Delta_0^2 \xi^2/(\epsilon_F a^2) \sim \epsilon_F$—in the clean limit[2] (with ϵ_F the Fermi energy). Hence, E_c is at a very high energy scale relative to T_c. Because the vortex unbinding temperature depends primarily on the stiffness term in K_s in Eq. (14) and is insensitive to E_c, this observation does not affect T_c. However, a large ratio $E_c/k_B T_c$ implies that the spontaneous vortex density should remain very small over a broad interval above T_c which is inconsistent with magnetization and transport experiments. The inconsistency has been used[2,27,30] to argue that the state stable inside the core is

actually much closer in energy to *d*SC than the true normal state (this is known as the cheap-vortex problem). Lee and co-workers propose that this is the sF state.[2,30]

As discussed in Sec. VIII, ρ rises very steeply above H_m to saturate near H_{ridge} long before H_{c2} is reached. Ioffe and Millis[88] have investigated how proximity to the Mott insulator influences the coupling between quasiparticles and the supercurrent and dissipation inside the vortex core. They propose that a small damping η results from the small number of states in the cores. The weak damping leads to a high velocity of the vortices transverse to **I** and a large flux-flow resistivity (or small vortex conductivity σ^s). Additivity of the vortex and qp charge currents[89] implies that, eventually, the observed conductivity $\sigma^s+\sigma^n$ is dominated by the qp term σ^n. This seems to account for the steep rise of ρ followed by rapid saturation.

Gaussian limit. As mentioned in Sec. III, phase fluctuations are classified as either analytical (spin-wave) $\Delta\theta_a$ or singular (vortex) $\Delta\theta_v$. The Gaussian-fluctuation theory, based on an expansion in small $|\Psi|$ of the action S, leaves out the essential role of $\Delta\theta_v$ in destroying superfluidity. Ussishkin *et al.*[43] have investigated the extent to which e_N^s measured in LSCO may be described by Gaussian theory applied to a generic layered, extreme type-II superconductor. In the 2D limit, they calculate that, above T_c, α_{xy}^s has the mean-field Aslamazov-Larkin (AL) form familiar from fluctuation diamagnetism—viz., $\alpha_{xy}^s \sim B(1-t)^{-1}$—which provides a reasonable fit to $e_N^s=\rho\alpha_{xy}^s$ in the OV regime [using the measured $\rho(T)$]. However, the Gaussian expression fits poorly in the OP and UD regimes even when unrealistically large values are used for the in-plane ξ.

Because Gaussian theory does not handle singular phase fluctuations and the phase-disordering scenario, it cannot describe the anomalous behavior of H_{c2} described above. The poor fits in the OP and UD regimes are perhaps unsurprising. However, in a restricted range of temperatures just below the curve of T_{onset} in Fig. 20 where amplitude fluctuations must be dominant it serves as a useful quantitative guide.[90] Numerical simulations of the 2D time-dependent Ginzburg Landau (TDGL) equation show reasonable fits to the high-field Nernst results in OV LSCO.[91]

The separate issue of whether any generic quasi-2D superconductor should display a large Nernst signal above T_c is interesting. The electron-doped NCCO, with an anisotropy and ρ comparable to OP LSCO and ξ_{ab} ($\sim$60 Å) 2.5 times larger, should display an even larger Nernst signal above T_c (according to the Gaussian theory). However, this is not the case (Sec. X). The presence or absence of the pseudogap state is a much more important discriminant in cuprates.

Quasiparticle models. We discuss some of the proposed models in which e_N above T_c is attributed to quasiparticles. It has been argued[35] that, if strong antiferromagnetic fluctuations exist in a Fermi liquid, vertex corrections cause the qp current $\mathbf{J_k}$ to deviate from being normal to the Fermi surface and a consequent enhancement of ν. Also, an enhanced qp ν is purportedly obtained in an unconventional *d*-density-wave (*d*DW) model,[36] as well as from paired holes in "antiphase" domains in an antiferromagnetic state.[38]

These models introduce a rather exotic qp property or ground state tailored to account for the Nernst data in a restricted interval of $T>T_c$, but ignore the (known) correlations of the data with other properties over a much larger parameter space. For example, it is difficult to see how the qp signal can smoothly evolve into the vortex signal below T_c (Fig. 13). It is equally difficult to imagine how the unusual qp states and properties abruptly cease to be effective once we move out of the T_c dome (Fig. 24). The extended high-field results reported here compound these problems. The vortex-hill profile which persists above T_c (Fig. 11), the scaling of e_N with M (Fig. 26), the anomalous behavior of H_{c2} (Fig. 13), and the contrasting case of NCCO (Fig. 28) all present serious challenges for the qp models. (Further, a recent calculation[86] has shown that the qp Nernst signal in the *d*DW state is actually too small to account for the observed e_N.)

Finally, in a proposed "bipolaron" model, even the Nernst signal observed *below* T_c has been identified as coming from ("localized") quasiparticles.[39] The extreme view is proposed that H_m represents the depairing field,[69] so that the condensate is destroyed as soon as ρ becomes nonzero. As we stressed in discussing ρ in Sec. VII, loss of phase stiffness should be carefully distinguished from the destruction of the condensate. The ubiquitous "tilted-hill" profile observed below T_c and the robustness of M observed to intense fields[53,81] provide simple, direct evidence refuting the basic assumption in this model.

XII. SUMMARY AND CONCLUSIONS

In the hole-doped cuprates, we uncover a large region above the "superconducting dome" in which an enhanced Nernst signal exists. The upper limit of the Nernst region is defined by T_{onset} which lies nominally half way between T_c and the pseudogap scale T^* (Sec. VIII). The Nernst signal is consistent in sign and magnitude with the phase-slip E field caused by a vortex current driven by the applied gradient (and incompatible with a ferromagnetic origin[44] by orders of magnitude). At each T within this region, the Nernst signal e_N is manifestly nonlinear in H and closely similar in shape to the tilted-peak profile that characterizes the vortex-Nernst signal observed below T_c (Sec. VI). This profile is strikingly incompatible with a qp origin, given the very short qp ℓ. Overall, the enhanced Nernst signal above T_c displays a smooth continuity with the vortex-liquid state below T_c, which is best seen in the contour plot of $e_N(T,H)$ in the T-H plane (Sec. VI).

An enhanced magnetization signal is observed above T_c that scales accurately with e_N measured in the same crystal (Sec. IX). The magnitude of M is significantly larger than that anticipated from Gaussian fluctuations. Moreover, it remains robust to intense fields like e_N even very near T_c. With the magnetization result, the vortex liquid above T_c has now been detected by both transport and thermodynamic experiments.

The direct implication of these results is that the loss of superfluidity and the collapse of the Meissner state at T_c occurs because long-range phase coherence is destroyed by

the thermal generation of vortices and antivortices, which implies that the pair amplitude $|\hat{\Psi}|$ persists to temperatures much higher than T_c. This phase disordering is the 3D analog of the KT transition in 2D systems.

For this scenario to be self-consistent, the depairing field H_{c2} must remain at a large finite value at T_c—as previously noted for the KT transition[13]—instead of decreasing to zero as $(1-T/T_c)$. Utilizing the vortex profile for e_N^s, we have determined that H_{c2} behaves anomalously, remaining large as T_c is crossed, consistent with the vortex scenario (Sec. VII). This implies that, in the plane (T,H), the critical point $(T_c,0)$ serves as the termination point of the melting-field curve $H_m(T)$, but not of the depairing field scale (Fig. 13). This contrasts with the phase diagram in NCCO (Fig. 28), in which $(T_c,0)$ serves as the termination point of both $H_m(T)$ and $H_{c2}(T)$. The latter is the canonical behavior in the BCS gap-closing scenario. The extension of the vortex liquid to above T_c, together with the anomalous behavior of H_{c2} constitute the most striking signatures of the phase-disordering scenario.

ACKNOWLEDGMENTS

We thank Z. Xu, Yoichi Ando, S. Ono, S. Uchida, Genda Gu, Y. Tokura, Y. Onose, B. Keimer, R. X. Liang, D. A. Bonn, and W. N. Hardy for helpful collaborations in these experiments. We are especially indebted to M. J. Naughton for drawing our attention to Ref. 77 and for the loan of cantilever magnetometers. We thank P. W. Anderson, J. C. Davis, D. A. Huse, S. A. Kivelson, P. A. Lee, K. Levin, A. J. Millis, V. N. Muthukumar, V. Oganesyan, J. Orenstein, S. Sachdev, S. Sondhi, Z. Tesanovic, I. Ussishkin, Z. Y. Weng, A. Yazdani, and S. C. Zhang for many helpful discussions. The high-field measurements were performed at the National High Magnetic Field Laboratory, Tallahassee, a facility supported by the U.S. National Science Foundation (NSF) and the State of Florida. We are grateful to Scott Hannahs for technical assistance. This research is supported by NSF (Grant No. DMR 0213706) and by the New Energy and Industrial Technology Development Organization (NEDO) (Japan).

*Present address: Department of Physics, University of California at Berkeley, Berkeley, CA 94720-7300, USA. Electronic address: yywang@berkeley.edu
†Electronic address: luli@princeton.edu
‡Electronic address: npo@princeton.edu

[1] For a review, see T. Timusk and B. Stratt, Rep. Prog. Phys. **62**, 61 (1999).
[2] For a review, see Patrick A. Lee, Naota Nagaosa, and Xiao-Gang Wen, Rev. Mod. Phys. **78**, 17 (2006).
[3] For a review, see E. W. Carlson, V. J. Emery, S. A. Kivelson, and D. Orgad, cond-mat/0206217 (unpublished).
[4] V. J. Emery and S. A. Kivelson, Nature (London) **374**, 434 (1995).
[5] G. Baskaran, Z. Zou, and P. W. Anderson, Solid State Commun. **63**, 973 (1987).
[6] S. Doniach and M. Inui, Phys. Rev. B **41**, 6668 (1990).
[7] H. J. Kwon and A. T. Dorsey, Phys. Rev. B **59**, 6438 (1999).
[8] V. B. Geshkenbein, L. B. Ioffe, and A. I. Larkin, Phys. Rev. B **55**, 3173 (1997).
[9] M. Franz and A. J. Millis, Phys. Rev. B **58**, 14572 (1998).
[10] J. M. Kosterlitz and D. J. Thouless, J. Phys. C **6**, 1181 (1973).
[11] J. Villain, J. Phys. (Paris) **36**, 581 (1975).
[12] M. R. Beasley, J. E. Mooij, and T. P. Orlando, Phys. Rev. Lett. **42**, 1165 (1979).
[13] S. Doniach and B. A. Huberman, Phys. Rev. Lett. **42**, 1169 (1979).
[14] B. I. Halperin and D. R. Nelson, J. Low Temp. Phys. **36**, 599 (1979).
[15] Y. Matsuda, S. Komiyama, T. Onogi, T. Terashima, K. Shimura, and Y. Bando, Phys. Rev. B **48**, 10498 (1993); H. J. Jensen, P. Minnhagen, E. Sonin, and H. Weber, Europhys. Lett. **20**, 463 (1992); J.-M. Triscone, P. Fivat, M. Andersson, M. Decroux, and Ø. Fischer, Phys. Rev. B **50**, 1229 (1994).
[16] J. Corson, R. Mallozzi, J. Orenstein, J. N. Eckstein, and I. Bozovic, Nature (London) **398**, 221 (1999).
[17] Y. J. Uemura, G. M. Luke, B. J. Sternlieb, J. H. Brewer, J. F. Carolan, W. N. Hardy, R. Kadono, J. R. Kempton, R. F. Kiefl, S. R. Kreitzman, P. Mulhern, T. M. Riseman, D. Ll. Williams, B. X. Yang, S. Uchida, H. Takagi, J. Gopalakrishnan, A. W. Sleight, M. A. Subramanian, C. L. Chien, M. Z. Cieplak, Gang Xiao, V. Y. Lee, B. W. Statt, C. E. Stronach, W. J. Kossler, and X. H. Yu, Phys. Rev. Lett. **62**, 2317 (1989); Y. J. Uemura, A. Keren, L. P. Lee, G. M. Luke, W. D. Wu, Y. Kubo, T. Manako, Y. Shimakawa, M. Subramanian, J. L. Cobb, and J. T. Markert, Nature (London) **364**, 605 (1993).
[18] Z. A. Xu, N. P. Ong, Y. Wang, T. Kakeshita, and S. Uchida, Nature (London) **406**, 486 (2000).
[19] Y. B. Kim and M. J. Stephen, in *Superconductivity*, edited by R. D. Parks (Dekker, New York, 1969), Vol. 2, p. 1107.
[20] Yayu Wang, Z. A. Xu, T. Kakeshita, S. Uchida, S. Ono, Y. Ando, and N. P. Ong, Phys. Rev. B **64**, 224519 (2001).
[21] Yayu Wang, N. P. Ong, Z. A. Xu, T. Kakeshita, S. Uchida, D. A. Bonn, R. Liang, and W. N. Hardy, Phys. Rev. Lett. **88**, 257003 (2002).
[22] Yayu Wang, S. Ono, Y. Onose, G. Gu, Y. Ando, Y. Tokura, S. Uchida, and N. P. Ong, Science **299**, 86 (2003).
[23] N. P. Ong and Yayu Wang, Physica C **408**, 11 (2004).
[24] N. P. Ong, Yayu Wang, S. Ono, Yoichi Ando, and S. Uchida, Ann. Phys. **13**, 9 (2004).
[25] C. Capan, K. Behnia, J. Hinderer, A. G. M. Jansen, W. Lang, C. Marcenat, C. Marin, and J. Flouquet, Phys. Rev. Lett. **88**, 056601 (2002).
[26] H. H. Wen, Z. Y. Liu, Z. A. Xu, Z. Y. Weng, F. Zhou, and Z. X. Zhao, Europhys. Lett. **63**, 583 (2003); Z. Wang, L. Shan, Y. Z. Zhang, J. Yan, F. Zhou, J. W. Xiong, W. X. Ti, and H. H. Wen, Phys. Rev. B **72**, 054509 (2005).
[27] P. A. Lee, Physica C **388**, 7 (2003).
[28] O. Vafek and Z. Tesanovic, Phys. Rev. Lett. **91**, 237001 (2003); A. Melikyan and Z. Tesanovic, Phys. Rev. B **71**, 214511 (2005).
[29] Z. Y. Weng and V. N. Muthukumar, Phys. Rev. B **66**, 094509 (2002); Z. C. Gu and Z. Y. Weng, *ibid.* **72**, 104520 (2005).
[30] C. Honerkamp and P. A. Lee, Phys. Rev. Lett. **92**, 177002 (2004).

[31] H. D. Chen, O. Vafek, A. Yazdani, and S. C. Zhang, Phys. Rev. Lett. **93**, 187002 (2004).
[32] S. Sachdev and E. Demler, Phys. Rev. B **69**, 144504 (2004).
[33] L. Balents, L. Bartosch, A. Burkov, S. Sachdev, and K. Sengupta, Phys. Rev. B **71**, 144508 (2005).
[34] P. W. Anderson, Phys. Rev. Lett. **96**, 017001 (2006).
[35] H. Kontani, Phys. Rev. Lett. **89**, 237003 (2002).
[36] B. Dora, K. Maki, A. Vanyolos, and A. Virosztek, Phys. Rev. B **68**, 241102(R) (2003).
[37] S. Tan and K. Levin, Phys. Rev. B **69**, 064510 (2004).
[38] C. R. Hu, Int. J. Mod. Phys. B **17**, 18 (2003).
[39] A. S. Alexandrov and V. N. Zavaritsky, Phys. Rev. Lett. **93**, 217002 (2004).
[40] C. Caroli and K. Maki, Phys. Rev. **164**, 591 (1967).
[41] K. Maki, Phys. Rev. Lett. **21**, 1755 (1968); J. Low Temp. Phys. **1**, 45 (1969).
[42] C. R. Hu, Phys. Rev. B **13**, 4780 (1976).
[43] I. Ussishkin, S. L. Sondhi, and D. A. Huse, Phys. Rev. Lett. **89**, 287001 (2002).
[44] Wei-Li Lee, S. Watauchi, V. L. Miller, R. J. Cava, and N. P. Ong, Phys. Rev. Lett. **93**, 226601 (2004).
[45] F. A. Otter and P. R. Solomon, Phys. Rev. Lett. **16**, 681 (1966); A. T. Fiory and B. Serin, *ibid.* **19**, 227 (1967).
[46] R. P. Huebener and A. Seher, Phys. Rev. **181**, 701 (1969); **181**, 710 (1969); V. A. Rowe and R. P. Huebener, *ibid.* **185**, 666 (1969).
[47] P. W. Anderson, Rev. Mod. Phys. **38**, 298 (1966).
[48] F. Vidal, Phys. Rev. B **8**, 1982 (1973).
[49] P. W. Anderson, Phys. Rev. **112**, 1900 (1958); **130**, 439 (1963).
[50] E. W. Carlson, S. A. Kivelson, V. J. Emery, and E. Manousakis, Phys. Rev. Lett. **83**, 612 (1999).
[51] V. Oganesyan, D. A. Huse, and S. L. Sondhi, cond-mat/0502224 (unpublished).
[52] S. Hikami and T. Tsuneto, Prog. Theor. Phys. **63**, 387 (1980).
[53] Lu Li, Yayu Wang, M. J. Naughton, S. Ono, Y. Ando, and N. P. Ong, Europhys. Lett. **72**, 451 (2005).
[54] K. Hirakawa and K. Ubukoshi, J. Phys. Soc. Jpn. **50** 1909 (1981).
[55] A. K. Nguyen and A. Sudbø, Phys. Rev. B **60**, 15307 (1999).
[56] J. P. Gollub, M. R. Beasley, R. Callarotti, and M. Tinkham, Phys. Rev. B **7**, 3039 (1973).
[57] M. Zeh, H. C. Ri, F. Kober, R. P. Huebener, A. V. Ustinov, J. Mannhart, R. Gross, and A. Gupta, Phys. Rev. Lett. **64**, 3195 (1990); H. C. Ri, R. Gross, F. Gollnik, A. Beck, R. P. Huebener, P. Wagner, and H. Adrian, Phys. Rev. B **50**, 3312 (1994).
[58] S. J. Hagen, C. J. Lobb, R. L. Greene, M. G. Forrester, and J. Talvacchio, Phys. Rev. B **42**, 6777 (1990).
[59] J. A. Clayhold, A. W. Linnen, Jr., F. Chen, and C. W. Chu, Phys. Rev. B **50**, 4252 (1994); J. A. Clayhold, *ibid.* **54**, 6103 (1996).
[60] T. T. M. Palstra, B. Batlogg, L. F. Schneemeyer, and J. V. Waszczak, Phys. Rev. Lett. **64**, 3090 (1990).
[61] D. S. Fisher, M. P. A. Fisher, and D. A. Huse, Phys. Rev. B **43**, 130 (1991).
[62] U. Welp, S. Fleshler, W. K. Kwok, R. A. Klemm, V. M. Vinokur, J. Downey, B. Veal, and G. W. Crabtree, Phys. Rev. Lett. **67**, 3180 (1991).
[63] S. Ullah and A. T. Dorsey, Phys. Rev. B **44**, 262 (1991).
[64] H. Ding, T. Yokoya, J. C. Campuzano, T. Takahashi, M. Randeria, M. R. Norman, T. Mochiku, K. Kadowaki, and J. Giapintzakis, Nature (London) **382**, 51 (1996).
[65] A. G. Loeser, Z. X. Shen, D. S. Dessau, D. S. Marshall, C. H. Park, P. Fournier, and A. Kapitulnik, Science **273**, 325 (1996).
[66] J. E. Hoffman, K. McElroy, D. H. Lee, K. M. Lang, H. Eisaki, S. Uchida, and J. C. Davis, Science **297**, 1148 (2002); J. E. Hoffman, E. W. Hudson, K. M. Lang, V. Madahavan, H. Eisaki, S. Uchida, and J. C. Davis, *ibid.* **295**, 466 (2002).
[67] M. Vershinin, S. Misra, S. Ono, Y. Ando, and A. Yazdani, Science **303**, 1995 (2004).
[68] A. P. Mackenzie, S. R. Julien, G. G. Lonzarich, A. Carrington, S. D. Hughes, R. S. Liu, and D. C. Sinclair, Phys. Rev. Lett. **71**, 1238 (1993); M. S. Osofsky, R. J. Soulen, Jr., S. A. Wolf, J. M. Broto, H. Rakoto, J. C. Ousset, G. Coffe, S. Askenazy, P. Pari, I. Bozovic, J. N. Eckstein, and G. F. Virshup, *ibid.* **71**, 2315 (1993).
[69] A. S. Alexandrov, V. N. Zavaritsky, W. Y. Liang, and P. L. Nevsky, Phys. Rev. Lett. **76**, 983 (1996).
[70] P. G. de Gennes, *Superconductivity of Metals and Alloys* (Addison Wesley, Reading, MA, 1989).
[71] J. M. Harris, Z. X. Shen, P. J. White, D. S. Marshall, M. C. Schabel, J. N. Eckstein, and I. Bozovic, Phys. Rev. B **54**, R15665 (1996).
[72] H. Ding, J. R. Engelbrecht, Z. Wang, J. C. Campuzano, S. C. Wang, H. B. Yang, R. Rogan, T. Takahashi, K. Kadowaki, and D. G. Hinks, Phys. Rev. Lett. **87**, 227001 (2001).
[73] Ch. Renner, B. Revaz, J.-Y. Genoud, K. Kadowaki, and Ø. Fischer, Phys. Rev. Lett. **80**, 149 (1998).
[74] S. H. Pan, E. W. Hudson, A. K. Gupta, K. W. Ng, H. Eisaki, S. Uchida, and J. C. Davis, Phys. Rev. Lett. **85**, 1536 (2000).
[75] J. L. Tallon and J. W. Loram, Physica C **349**, 53 (2001).
[76] M. R. Presland, J. L. Tallon, R. G. Buckley, R. S. Liu, and N. E. Flower, Physica C **176**, 95 (1991).
[77] M. J. Naughton, Phys. Rev. B **61**, 1605 (2000).
[78] C. Bergemann, A. W. Tyler, A. P. Mackenzie, J. R. Cooper, S. R. Julian, and D. E. Farrell, Phys. Rev. B **57**, 14387 (1998).
[79] A. Lascialfari, A. Rigamonti, L. Romano, A. A. Varlamov, and I. Zucca, Phys. Rev. B **68**, 100505(R) (2003).
[80] C. Carballeira, J. Mosqueira, R. Revcolevschi, and F. Vidal, Phys. Rev. Lett. **84**, 3157 (2000).
[81] Yayu Wang, Lu Li, M. J. Naughton, G. D. Gu, S. Uchida, and N. P. Ong, Phys. Rev. Lett. **95**, 247002 (2005).
[82] R. Bel, K. Behnia, and H. Berger, Phys. Rev. Lett. **91**, 066602 (2003).
[83] H. Balci, C. P. Hill, M. M. Qazilbash, and R. L. Greene, Phys. Rev. B **68**, 054520 (2003).
[84] Z. Z. Wang, T. R. Chien, N. P. Ong, J. M. Tarascon, and E. Wang, Phys. Rev. B **43**, 3020 (1991).
[85] P. Fournier, X. Jiang, W. Jiang, S. N. Mao, T. Venkatesan, C. J. Lobb, and R. L. Greene, Phys. Rev. B **56**, 14149 (1997).
[86] V. Oganesyan and I. Ussishkin, Phys. Rev. B **70**, 054503 (2004).
[87] P. A. Lee and X. -G. Wen, Phys. Rev. B **63**, 224517 (2001).
[88] L. B. Ioffe and A. J. Millis, Phys. Rev. B **66**, 094513 (2002).
[89] J. M. Harris, N. P. Ong, P. Matl, R. Gagnon, L. Taillefer, T. Kimura, and K. Kitazawa, Phys. Rev. B **51**, R12053 (1995).
[90] I. Ussishkin and S. L. Sondhi, cond-mat/0406347 (unpublished); I. Ussishkin, Phys. Rev. B **68**, 024517 (2003).
[91] S. Mukerjee and D. A. Huse, Phys. Rev. B **70**, 014506 (2004).